ARTICLES
https://doi.org/10.1038/s41929-022-00771-w

nature catalysis

Check for updates

Ground-state destabilization by electrostatic repulsion is not a driving force in orotidine-5′-monophosphate decarboxylase catalysis

Sören Rindfleisch[1,2,7], Matthias Krull[3,7], Jon Uranga[4,7], Tobias Schmidt[3], Fabian Rabe von Pappenheim[1,2], Laura Liliana Kirck[1,2], Angeliki Balouri[4], Thomas Schneider[5], Ashwin Chari[2], Ronald Kluger[6], Gleb Bourenkov[5], Ulf Diederichsen[3,8], Ricardo A. Mata[4] ✉ and Kai Tittmann[1,2] ✉

The origins of enzyme catalysis have been attributed to both transition-state stabilization as well as ground-state destabilization of the substrate. For the latter paradigm, the enzyme orotidine-5′-monophosphate decarboxylase (OMPDC) serves as a reference system as it contains a negatively charged residue at the active site that is thought to facilitate catalysis by exerting an electrostatic stress on the substrate carboxylate leaving group. Snapshots of how the substrate binds to the active site and interacts with the negative charge have remained elusive. Here we present crystallographic snapshots of human OMPDC in complex with the substrate, substrate analogues, transition-state analogues and product that defy the proposed ground-state destabilization by revealing that the substrate carboxylate is protonated and forms a favourable low-barrier hydrogen bond with a negatively charged residue. The catalytic prowess of OMPDC almost entirely results from the transition-state stabilization by electrostatic interactions of the enzyme with charges spread over the substrate. Our findings bear relevance for the design of (de)carboxylase catalysts.

Orotidine-5′-monophosphate decarboxylase (OMPDC) serves as a paradigm for our understanding of how enzymes catalyse chemical reactions[1–4]. It catalyses the decarboxylation of orotidine-5′-monophosphate (OMP) to uridine-5′-monophosphate (UMP) in the de novo biosynthesis of pyrimidine nucleotides in all domains of life (Fig. 1a). OMPDC is one of the most proficient enzyme catalysts known and exhibits a remarkable rate enhancement of 17 orders of magnitude compared with that of the uncatalysed reaction, which reduces the half-life from 78 million years to the milliseconds regime[1]. Intriguingly, it does so without the involvement of metal ions, bioorganic cofactors or prosthetic groups. Instead, OMPDC relies on a few polar residues at the active site, which include the catalytic tetrad that consists of two aspartate and two lysine residues[5–8]. This seemingly simple active-site configuration in combination with the enormous rate enhancement has sparked intense research into the governing principles of OMPDC catalysis. Despite these efforts and numerous mechanistic proposals, the enzymatic mechanism of OMPDC is still enigmatic (Extended Data Fig. 1)[1–8]. The kinetic bottleneck of the reaction is the required stabilization of an evolving carbanion in the transition state that cannot be stabilized by delocalization as, for example, in cofactor enzymes. It is difficult to gather consensus around the origin of the catalytic prowess of OMPDC. One possibility is the transition-state stabilization of a localized vinyl carbanion by a positively charged lysine residue[3,4,9] that also serves as the bona fide acid–base catalyst for quenching the incipient carbanion by protonation. Concurrently, it is proposed that substrate ground-state destabilization by a negatively aspartate residue also takes place. The latter would electrostatically stress the equally charged substrate carboxylate leaving group, and thus promote expulsion of the uncharged carbon dioxide product (Fig. 1a,b)[3,5,10]. The thermodynamic penalty associated with this unfavourable, repulsive interaction between enzyme and substrate was proposed to be paid by a favourable binding of non-reacting substrate parts (5′-monophosphate and ribose portions), a concept known as the Circe effect in enzymology[11]. This proposal has been met with strong criticism, in particular from Warshel and co-workers who employed computational calculations and suggested a mechanism that prevalently relies on transition-state stabilization[12–14]. A recent mechanistic study also proposed transition-state stabilization as the main driving force of OMPDC catalysis[15]. Although these mechanistic proposals are intuitive and chemically reasonable, they remained hypothetical as the structural basis of OMPDC catalysis is still elusive in several critical aspects. For one, the atomic structure of a substrate OMP bound to the active site of OMPDC and its interaction with the stressing aspartate is unknown, as so far structures are only available for OMPDC variants in which the stressing aspartate had been replaced[16,17]. Second, tight-binding transition-state analogues, such as 6-hydroxy-UMP (BMP) or 6-aza-UMP as mimics for the proposed carbanion were identified (Fig. 1c) and structures of these

[1]Department of Molecular Enzymology, Göttingen Center of Molecular Biosciences, Georg-August University Göttingen, Göttingen, Germany. [2]Department of Structural Dynamics, Max-Planck-Institute for Biophysical Chemistry, Göttingen, Germany. [3]Institute for Organic and Biomolecular Chemistry, Georg-August University Göttingen, Göttingen, Germany. [4]Institute of Physical Chemistry, Georg-August University Göttingen, Göttingen, Germany. [5]European Molecular Biology Laboratory (EMBL), Hamburg Outstation c/o Deutsches Elektronen Synchrotron (DESY), Hamburg, Germany. [6]Department of Chemistry, University of Toronto, Ontario, Canada. [7]These authors contributed equally: Sören Rindfleisch, Matthias Krull, Jon Uranga. [8]This publication is dedicated to our collaborator, colleague and friend Ulf Diederichsen (1963–2021). ✉e-mail: rmata@gwdg.de; ktittma@gwdg.de

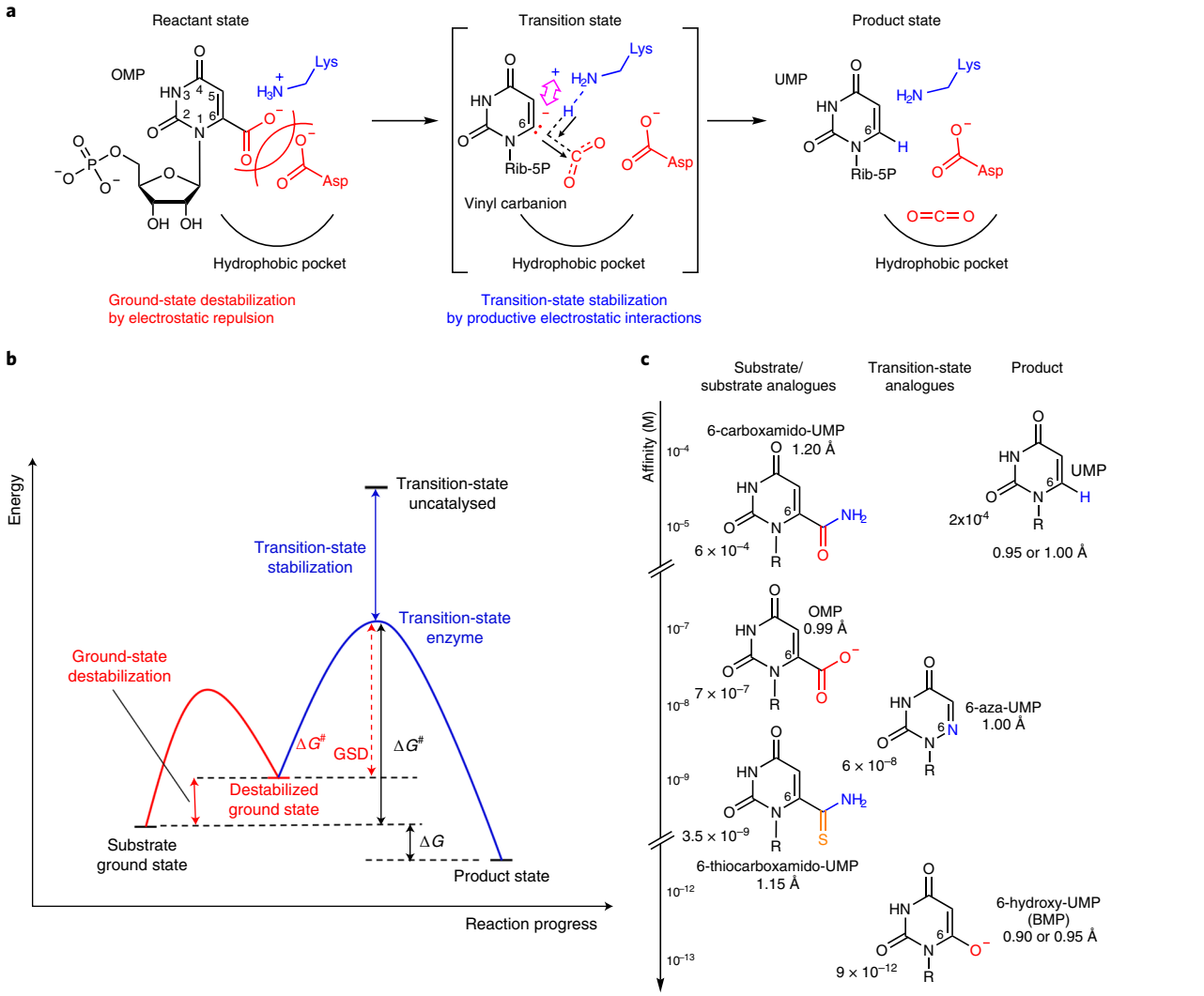

Fig. 1 | Proposed mechanism and catalytic strategies of OMPDC. a, Currently accepted mechanism of OMPDC action, which invokes ground-state destabilization by electrostatic repulsion between the substrate carboxylate and an active site aspartate and transition-state stabilization by a lysine that electrostatically stabilizes the vinyl carbanion and acts as a general acid. **b**, Energy profile of the OMPDC-catalysed reaction indicating the proposed ground-state destabilization and transition-state stabilization. ΔG, free-energy change; $\Delta G^{\#}$, activation energy; $\Delta G^{\#}_{GSD}$, activation energy starting from the destabilized ground state. **c**, Chemical structures of substrate and substrate analogues, transition-state analogues and products, and the experimentally determined affinities for yeast OMPDC as a reference system[3]. The resolution of X-ray crystallographic structures of human OMPDC in complex with these compounds (this study) is indicated in each case.

bound to OMPDCs were determined[3–10,12,13]. However, the charge configuration and protonation state of both the transition-state analogue and surrounding active-site residues have remained elusive as this requires ultrahigh-resolution X-ray crystallographic data[18], a prerequisite not met in previous studies.

Here, we close this gap of knowledge and unveil the structural basis of OMPDC catalysis by determining ultrahigh-resolution X-ray structures of the human enzyme in complex with the genuine substrate OMP, the highest-affinity substrate analogues, the highest-affinity transition-state analogues and the product UMP. In case of the genuine substrate, we reached temporal resolution (Fig. 1c). The novel structural information was combined with quantum chemical calculations to define the basis of OMPDC catalysis, and necessitated a revision of the accepted mechanism with implications for our general understanding of enzyme action. In addition, we report on the detection of the hitherto unknown cooperativity of the homodimeric OMPDC on both the structural and functional levels.

Results

Structure of the enzyme substrate complex. Owing to the fleeting existence of OMP in the enzyme-bound state and its rapid turnover to UMP in OMPDC crystals, substrate soaking of wild-type enzyme crystals is not suited to structurally visualize the bound substrate as the product UMP is almost instantly accumulated (in our hands, in just a couple of minutes). Substitutions of residues that belong to the catalytic tetrade by canonical amino acids turned out to be detrimental to the active-site geometry as the charge and hydrogen-bond network collapsed[16,17]. We therefore opted to introduce a non-canonical near-native amino acid, for which key interactions at the active site would probably be preserved. Specifically, we replaced the catalytic Lys314 (Lys93 in yeast OMPDC and Lys72 in the OMPDC of *Methanobacterium thermoautotrophicum*) by its acetylated counterpart (Ac-Lys314) using the Schultz method[19]. The lysine side-chain skeleton, which included the Nζ atom, was maintained; however, the positive charge as well as the ability to act as an acid–base catalyst were eliminated, potentially

stalling catalysis. In fact, the catalytic activity of the human OMPDC variant Lys314Ac-Lys was almost completely abolished with a k_{cat} of $(2.0 \pm 0.3) \times 10^{-3}\,s^{-1}$, which corresponds to a residual activity of 0.06% compared with that of the wild type ($3.20 \pm 0.04\,s^{-1}$), whereas the substrate affinity ($K_M = 5.3 \pm 0.7\,\mu M$) was only slightly decreased (wild-type K_M of $1.5 \pm 0.1\,\mu M$). This suggests a predominant role of Lys314 in the transition-state stabilization (~4.4 kcal mol^{-1}). We then determined the structures of the variant in the resting state and in complex with the product UMP. The structural analyses confirmed the replacement of Lys314 by Ac-Lys and further revealed that the overall structure, which included that of the active site, was virtually unchanged compared with that of the wild-type situation, with the exception of a small flip around the Cδ–Cε bond of Ac-Lys314 (Extended Data Fig. 2). Next, we soaked the crystals of the AcK variant with substrate OMP with the goal to structurally visualize the enzyme-bound substrate. In fact, OMP accumulated in crystallo in the minutes time regime (2–30 min) with the highest occupancy at a 2 min soaking time (75% occupancy). We solved the structure of the OMPDC:OMP complex at a resolution of 0.99 Å using anisotropic processing (Fig. 2a). A well-defined electron density was observed for the whole substrate molecule, which allowed a reliable modelling of its conformation. The most surprising feature was a short, strong hydrogen bond of the carboxylate group with residue Asp312 (hydrogen-bond distance of 2.53 Å). Rather than being stressed by Asp312 (Asp91 in yeast OMPDC and Asp70 in the OMPDC of *M. thermoautotrophicum*), substrate OMP was engaged in a productive interaction with this residue and shared a proton in a dicarboxylate motif. Warshel and co-workers had previously pointed to the fact that the potential destabilization of the orotate is capped. At a certain point, depending on the pH and the strength of the interaction, one would observe protonation, which is energetically favoured (their estimates indicated a maximum penalty of 6.7 kcal mol^{-1} at pH 7 (ref. [13])). Both the 2mFo–DFc (Fo, observed diffraction data; Fcm, calculated diffraction data; *m*, figure of merit; D, Sigma-A weighting factor) electron density map and the estimated bond length of the substrate carboxylate C–O bonds suggested that the shared proton was more localized to the substrate. In fact, the estimated bond lengths were almost identical to those reported for protonated orotic acid characterized by small-molecule X-ray crystallography (Supplementary Fig. 1)[20]. The scissile C6–C7 bond of enzyme-bound OMP was physically distorted and exhibited an out-of-plane distortion of 21° relative to the base pyrimidine ring plane (Fig. 2b). Also, the plane of the substrate carboxylate was twisted by 43°, which reduced its conjugation with the π electrons of the pyrimidine. This distortion and twist were absent for free orotic acid, which suggests that the enzyme selectively destabilized the scissile substrate bond (Supplementary Fig. 1). The scissile C6–C7 bond (1.47 Å) was not elongated, as found for covalent substrate–cofactor intermediates[21,22], and exhibited a regular bond length similar to that reported for the free compound (1.50 Å). At the given resolution and OMP B-factors, the coordinate error as judged by the estimated s.d. of the calculated bond lengths amounted to ~0.01–0.02 Å (refs. [21,23]). Quantum chemical calculations (dihedral scans of the isolated orotic and orotate molecules) showed that distortions such as those observed in OMPDC bring about an energy penalty of roughly 2 kcal mol^{-1} (Supplementary Fig. 2). This far from fully explains the catalytic action of the system. Similar distortions and twists were detectable for the enzyme-bound substrate analogues 6-thiocarboxamido-UMP (substrate analogue with the highest affinity) and the related 6-carboxamido-UMP (Fig. 1c and Extended Data Fig. 3).

Since the X-ray structure with the bound substrate was determined for variant Lys314Ac-Lys, we restored the wild-type active site in silico and performed molecular dynamics simulations to test the relevance of the structural findings (Fig. 2c). Most importantly, the productive interaction between the substrate and Asp312 was retained; in fact, a low-barrier hydrogen bond between the two formed (Supplementary Fig. 3). The side chain of Lys314 did not interact with the substrate carboxylate but formed hydrogen bonds with Asp312, Asp317′ and the 2′-OH group of the substrate ribose portion, similar to what we observed in the experimentally determined structures of the OMPDC wild type in complex with substrate analogues (Extended Data Fig. 3). This rationalized our aforementioned finding of a major role of Lys314 for catalysis but minor role for substrate binding. The quantum mechanics/molecular mechanics (QM/MM) umbrella sampling calculations provided an estimate for the decarboxylation barrier of 13.8 kcal mol^{-1}, in very close agreement with the experimentally derived barrier of 15.3 kcal mol^{-1} (Fig. 2d). The underlying QM/MM dynamics suggest a mechanism in which synchronized proton transfers that involve the substrate, and residues Asp312 and Lys314 take place (Fig. 2e) to catalyse the protonation of the incipient carbanion at position 6 of the substrate. These proton jumps involve the whole tetrad, with several transfer events observed for Lys281, Asp312 and Lys314 (with Asp317 interacting favourably with the added proton charge in Lys314). This reaches the point at which it is actually difficult to assign specific stable protonation states to the aforementioned residues for each simulation window.

Time-resolved snapshots of OMPDC catalysis. Next, we analysed the structures of OMPDC variant Lys314Ac-Lys with substrate OMP at different time points to visualize the conversion of the substrate into the product UMP with temporal resolution. Prior to this analysis, we conducted dose-dependent experiments to study the impact of the high-energy synchrotron radiation on OMPDC crystals as a putative radiation damage may lead to non-enzymatic decarboxylation of enzyme-bound OMP[24]. We collected individual X-ray datasets with calibrated doses between 0.71 and 3.55 MGy on OMPDC crystals (soaked with substrate OMP for two minutes) and determined the individual structures of the enzyme–substrate complex (Extended Data Fig. 4). No radiation damage was detectable for the substrate OMP and the interacting amino acid residues at the active site for the dose range tested. We then analysed the structures of OMPDC soaked with substrate OMP for different time points that ranged from 2 to 30 minutes (Extended Data Fig. 5). Interestingly, the $C222_1$ space group obtained for the two-minute soak crystals (one monomer in the asymmetric unit) changed to space group $P2_1$ (functional dimer in the asymmetric unit) for longer soaking times, which indicates a loss of internal symmetry and non-equivalence of the two subunits of the dimer. Our structural analysis for these datasets revealed different occupancies with substrate OMP in the two active sites of the functional dimer and suggested a cooperativity between the two subunits. To test this hypothesis at the functional level, we conducted a steady-state kinetic analysis of OMPDC catalysis by isothermal titration calorimetry and, indeed, detected a positive cooperativity with a Hill coefficient n_H of 2.0, which was unknown for this protein (Extended Data Fig. 6a). The binding of product UMP to OMPDC was also governed by cooperativity between the two subunits, in this case a mild negative cooperativity, in which the estimated dissociation constants differed by approximately one order of magnitude for the two active sites (Extended Data Fig. 6b). The detection of negative cooperativity for the binding of substrate or product and positive cooperativity for steady-state turnover conditions is reminiscent of cofactor-dependent enzymes, which also form functional dimers with two active sites that are synchronized through a proton wire that spans from one active site to the other[25–27]. In the case of OMPDC, we could identify several putative communication pathways that consisted of acidic side chains and water molecules that could, in principle, fulfil a similar function (Extended Data Fig. 6c). Molecular dynamics calculations show that changes in the protonation state of one active site impacts the structure in the other monomer (even residues more than 30 Å away).

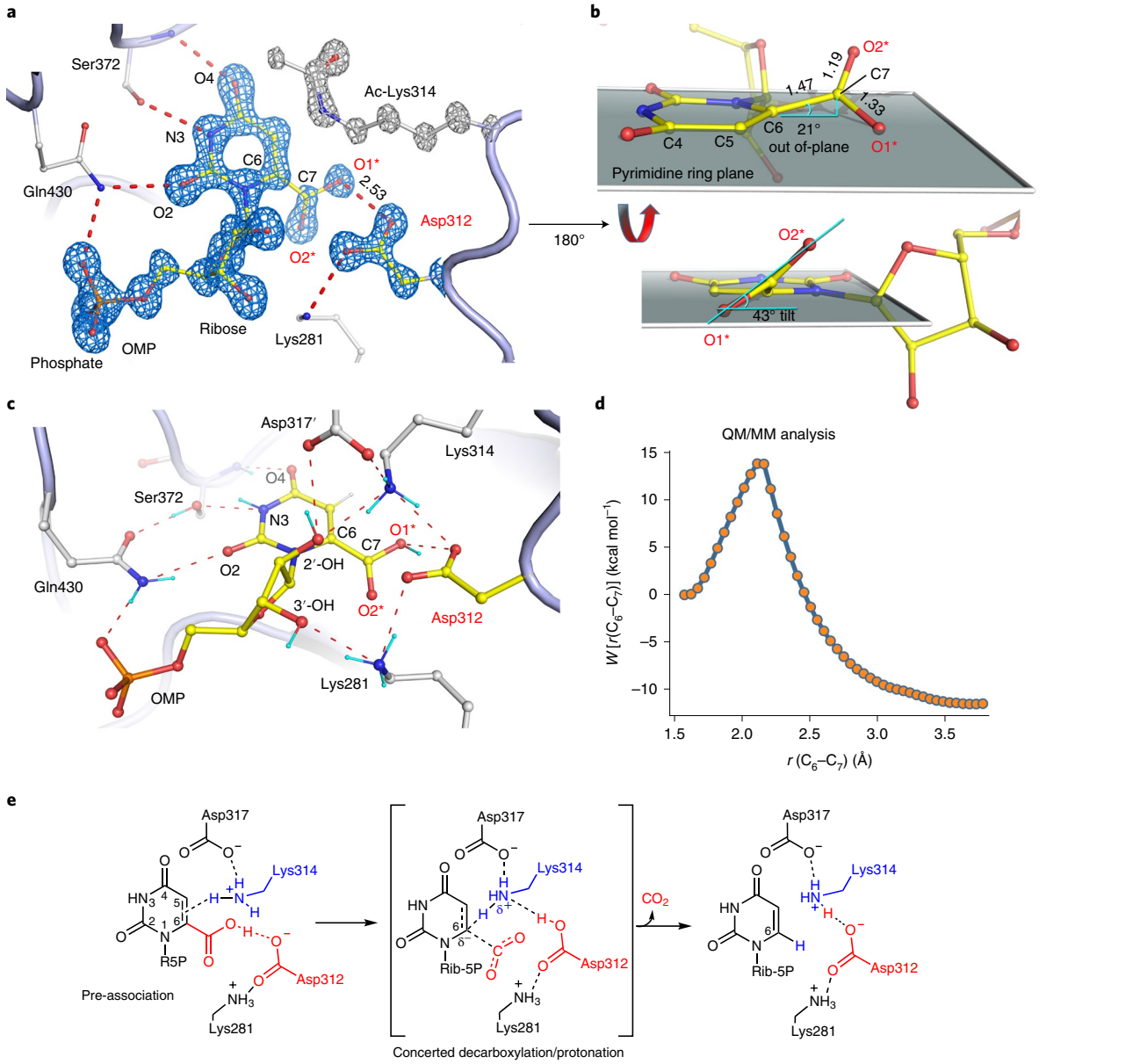

Fig. 2 | Structural snapshots of substrate binding in OMPDC. a, Structure of substrate OMP bound to the human OMPDC variant Lys314AcLys at a 0.99 Å resolution highlighting the critical hydrogen-bond interactions with protein groups. Note the short (2.53 Å), strong hydrogen bond between the substrate carboxylate and residue Asp312, which is incompatible with the proposed electrostatic repulsion between the two carboxylate groups. The structural models of substrate OMP, interacting residue Asp312 and mutated residue 314 are superposed with the corresponding 2mFo–DFc electron density map at a contour level of 3σ. **b**, Structural features of enzyme-bound OMP highlighting the out-of-plane distortion of the scissile C6–C7 bond and of the substrate carboxylate relative to the pyrimidine ring plane shown in grey, which suggest a selective bond activation of the scissile substrate bond. The estimated bond lengths for the scissile C6–C7 bond and the C–O bonds of the carboxyl moiety are indicated and suggest the substrate to be protonated at O1* (the structural features and bond lengths of free orotic acid are shown for comparison in Supplementary Fig. 1). The scissile C6–C7 bond is not elongated as, for example, observed in enzymic covalent substrate–cofactor conjugates[21]. **c**, Structure of the wild-type OMPDC active site with bound OMP obtained by QM/MM calculations after the in silico restoration of residue Lys314 using the experimentally determined X-ray structure of variant Lys314AcLys. Note the retained short, strong hydrogen bond between the substrate carboxylate and Asp312. Further, Lys314 is triangulated by hydrogen-bond interaction with Asp312, Asp317′ and the 2′-OH group of the substrate ribose, but is not interacting with the substrate. **d**, Potential of mean force (PMF) profile derived from umbrella sampling QM/MM calculations with the C6–C7 distance as a restraint (approximate reaction coordinate) for the decarboxylation reaction. The orange dots provide the PMF energies at the computed windows (spline interpolation in blue). **e**, Suggested mechanism of OMPDC catalysis based on the QM/MM calculations. Residues of the catalytic tetrad form an intimately coupled network of charged residues (Asp312$^-$/Lys281$^+$ and Lys314$^+$/Asp317′$^-$) with transient proton transfers. On substrate binding, Asp312 and the substrate carboxylate form a hydrogen bond with an additional proton (vide supra). In the transition state, synchronized proton transfers between substrate O1*, Asp312, Lys314 and the C6 position of the substrate take place to afford product UMP (see main text).

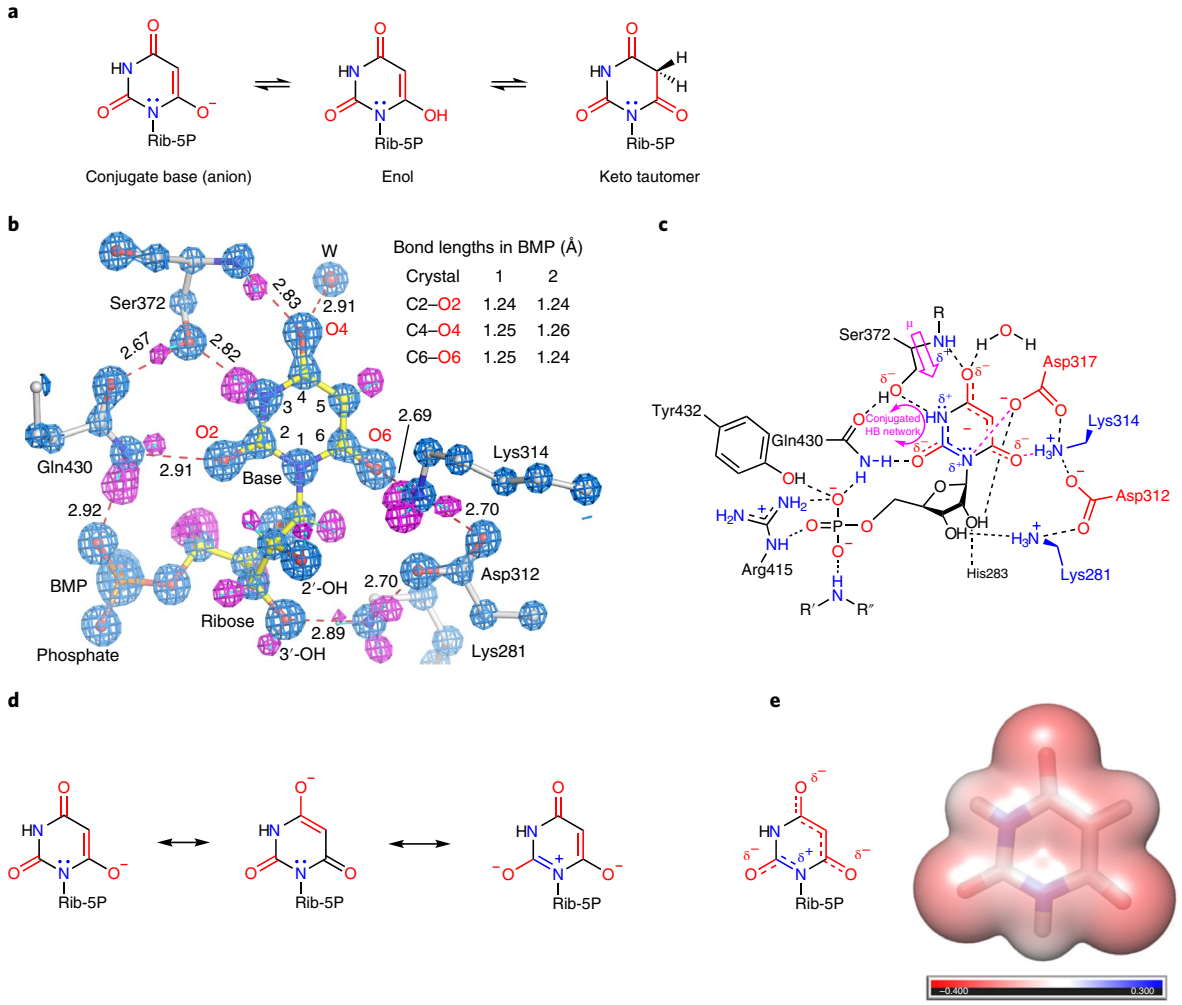

Fig. 3 | Structure of the transition-state analogue BMP bound to human OMPDC. a, Chemical structure of BMP showing the protonic and tautomeric equilibria. The conjugate base (enolate anion) has been suggested to be stabilized by OMPDC as a mimic of the vinyl carbanion rather than the charge neutral enol or the keto tautomer. **b**, Structure of BMP bound to the active site of human OMPDC at a resolution of 0.90 Å highlighting critical hydrogen-bonding interactions with protein groups. The structural model is superposed with the corresponding 2mFo–DFc electron density map (blue, contour level 5.3σ). Peaks in the hydrogen-omit mFo–DFc difference electron density map (magenta, contour level 3σ) indicate the positions of hydrogen atoms shown in cyan. The bond length of the C2–O2, C4–O4 and C6–O6 bonds of the base are indicated for both the structures determined in this study and indicate the accumulation of the anion form of BMP with a distribution of the negative charge rather than as a localized charge. **c**, Suggested chemical and electronic structure of OMPDC-bound BMP showing the corresponding ionization states as well as hydrogen-bond and electrostatic interactions. Note the spread of charge over the base, stabilizing charges (in magenta) and hydrogen bonds. **d**, Putative resonance contributors of OMPDC-bound BMP. **e**, Molecular electrostatic potential (MEP) of BMP (isosurface value of 0.005 e Bohr^{-3}, colour coding scale in atomic units) computed at the B3LYP-D3(BJ)/def2-SVP(IEPFPCM) level of theory. HB, hydrogen bonding.

This mechanism of signal propagation between the two chains bear similarities to the proton wire that operates in some cofactor enzymes (Supplementary Fig. 4)[25–27].

Structure with transition-state analogues. The transition-state analogue with the highest known affinity for OMPDC is BMP ($K = 9 \times 10^{-12}$ M), and it has been suggested that it is bound as the conjugate base with the 6-hydroxy function being deprotonated as a mimic of the postulated carbanion-type transition state (Fig. 3a)[3,7]. Although this is a reasonable proposal, the discrete protonation and tautomeric states of enzyme-bound BMP have not been characterized at the structural level. We solved two ultrahigh-resolution X-ray structures of the human OMPDC wild type in complex with BMP at resolutions of 0.90 and 0.95 Å. In both datasets, the protonation states of both the bound analogue and of all the interacting protein groups were unambiguously and completely assigned (Fig. 3b,c). None of the three base oxygen atoms (O2, O4 and O6) was found to be protonated and the estimated bond lengths for the C2–O2, C4–O4 and C6–O6 bonds were almost identical, which indicates that BMP was bound as a monoanion with the negative charge spread over the base. The charge configuration of the catalytic tetrad can be assigned as a network of alternating charges, Lys281$^+$–Asp312$^-$–Lys314$^+$–Asp317$^-$. The key catalytic residue Lys314 electrostatically interacts with the 6-O atom, in support of its suggested role for transition-state stabilization[3–8,16,17], and is firmly held in place by interactions with Asp312 and Asp317. It is perfectly oriented to protonate the evolving carbanion at C6 in the native reaction and thus block the internal return of CO_2 (refs. [28,29]). The 4-O atom of BMP interacts with the backbone amide of Ser372 and a water molecule, whereas O2 forms a hydrogen bond with the carboxamide function of Gln430 as part of a highly conjugated network that involves Ser372, Gln430 and the C2–O2 and N3–H

groups of BMP. Residue Asp317, which is contributed by the second subunit, sits atop the N1 atom of the base and could also be involved in charge stabilization (Extended Data Fig. 7). Apparently, OMPDC has evolved an effective transition-state stabilization by an architecture that provides multiple favourable electrostatic interactions in a network of alternating charges, as also supported by our quantum chemical calculations and mechanistic studies (Fig. 3d,e)[3–10,30]. The transition-state analogue with the second-highest affinity was 6-aza-UMP ($K = 6 \times 10^{-8}$ M) and this high affinity has been attributed to a similar configuration to that of the genuine transition state owing to the lone pair at N6[3]. We solved the X-ray crystallographic structure of that human OMPDC wild type in complex with 6-aza-UMP at a resolution of 1.00 Å (Extended Data Fig. 8). Intriguingly, the base adopts the *syn*-conformation as opposed to that adopted by all the other analogues, substrate and product, in which the *anti*-conformation is stabilized on the enzyme. As a consequence, the 2-oxo group faces a catalytic tetrad rather than Gln430, and forms an extended hydrogen-bond network with these residues and numerous solvent molecules. The estimated bond lengths suggest a higher degree of polarization of the C4–O4 bond compared with that of the C2–O2 bond, although the interaction of O4 with Ser372 is disengaged. Thus, it appears that the high affinity of OMPDC for 6-aza-UMP is not necessarily related to a binding scenario that resembles the genuine transition state.

Structure with the product and implications for the mechanism. We determined two structures of human OMPDC in complex with the product UMP at resolutions of 0.95 and 1.00 Å (Fig. 4a), which revealed identical geometries of UMP. In case of the 0.95 Å structure, we could even assign the protonation state of the base and ribose portions. The base was not ionized at position 6 and neither O2 nor O4 were protonated, although the estimated bond lengths suggest a slightly larger polarization of the C4–O4 bond (1.26 Å in both structures) compared with those of the C2–O2 bonds (1.21 and 1.23 Å, respectively). The spatial proximity and suitable orientation of Lys314 relative to the C6 position supports the notion that Lys314 protonates the incipient carbanion formed in the transition state. Both Lys314 and the neighbouring Asp317′ show alternative conformations, which suggests that the enzyme lost some grip in the product-bound state compared with that in the transition state, as also evidenced by the increased hydrogen-bond distances of, for example, the 4-oxo group of UMP with Ser372 and a water molecule (compare with Fig. 3). Taken together, the structural analysis of OMPDC in complex with the substrate OMP, transition state analogue BMP and product UMP reveals the basis for the differential bindings of the reactant and transition state (Fig. 4b). Both the substrate and the product are bound with no charge at the base portion, whereas a negative charge evolves in the transition state that is effectively stabilized by complementary (partial) charges, dipoles and/or hydrogen bonds interacting with functional groups of the base. Residue Asp312, previously suggested to stress the substrate carboxylate, is an essential element of the catalytic apparatus for a favourable binding of the substrate in the protonated, uncharged form. If the substrate were bound in the ionized, negatively charged state, the catalytic efficiency of OMPDC would, in large part, become lost as this requires a preferential binding of the transition state, which OMPDC accomplishes by selective stabilization of charges in the transition state only. This is further corroborated by functional and structural analysis of an Asp312Asn variant that we generated. This variant exhibited no measurable enzymatic activity (decarboxylation of OMP), as also reported by others[17]. The variant was, however, not deficient in binding substrate and product, as revealed by isothermal titration calorimetry (ITC) experiments (Extended Data Fig. 9). Our structural analysis of this variant in complex with substrate OMP obtained by crystal soaking showcases that the enzyme formed an overly stable substrate complex,

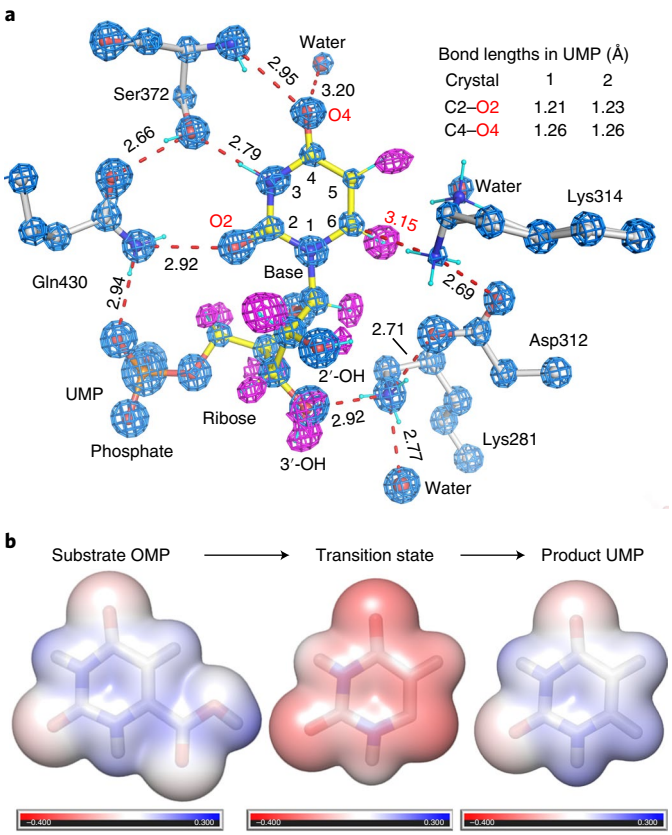

Fig. 4 | Structure of the product UMP bound to human OMPDC and implications for the mechanism. a, The structure of UMP bound to the active site of human OMPDC at a resolution of 0.95 Å highlights critical hydrogen-bonding interactions with protein groups. The structural model of UMP is superposed with the corresponding 2mFo–DFc electron density map (blue, contour level 5σ). Peaks in the hydrogen-omit mFo–DFc difference electron density map (magenta, contour level 2.5σ) indicate the positions of hydrogen atoms shown in cyan. The N3-bound hydrogen of UMP can be traced at lower contour levels. The bond lengths of C2–O2 and C4–O4 of the base are indicated for both structures determined in this study and indicate a slightly higher charge density at position 4. **b**, MEPs (isosurface value of 0.005 e Bohr^{-3}, colour coding scale in atomic units) for substrate OMP, the transition state and UMP computed at the B3LYP-D3(BJ)/def2-SVP(IEPFPCM) level of theory suggest that the catalytic prowess of OMPDC—its preferential binding of the transition state—mostly results from the development and spread of charge in the transition state and the charge stabilization by protein groups in addition to acid–base catalysis provided by the pre-associated general acid Lys314 (see main text).

in which both lysines of the tetrad (Lys314 and Lys281) electrostatically interact with the substrate carboxylate. Apparently, this strong reactant-state stabilization is anticatalytic and highlights the importance of residue Asp312 for masking the charge of the substrate in the reactant state. Residue Lys314 on the other hand is key to the stabilization of the carbanion in the transition state (although the extent of charge development remains to be characterized), but is not directly involved in binding of the substrate carboxylate, as this would potentially stabilize the ionized, negatively charged substrate and thus be detrimental for the required preferential binding of the transition state. Its positioning close to the decarboxylation site C6 at the opposite structural face where CO_2 is likely to depart suggests an 'enforced' pre-association mechanism with a concerted protonation and decarboxylation[31]. This would ensure the forward commitment of the reaction as the almost barrierless internal return of

CO_2 would be blocked[28,29]. The here uncovered governing principles of OMPDC catalysis may be useful for the design of enzymatic or synthetic CO_2-fixing catalysts[29,32–35].

Conclusions

Our structural analysis of OMPDC catalysis has unexpectedly revealed that an electrostatic repulsion between the substrate and enzyme, as one proposed form of ground-state destabilization[5,10,36], is not a driving force of this reaction. Although enzymes are capable of stressing their substrates by binding them in physically distorted conformations and thus selectively destabilize scissile substrate bonds, as demonstrated here and for other systems[18,21,22,37], electrostatic interactions are exploited productively and are central to effective transition-state stabilization as put forward in the theoretical concepts by Warshel and others[12–14,38–40]. The active site architecture of OMPDC, one of the most proficient enzymes[1–4], highlights the use of a network of alternating charges and dipoles that perfectly embrace the reacting substrate and stabilize the charges that evolve in the transition state and further provides a pre-associated proton[31] in the transition state of decarboxylation as part of a multisite proton relay that involves the substrate and catalytic tetrad. Enzymic decarboxylation is facilitated by hydrogen-bond interactions between the substrate carboxylate and acidic side chains of the protein that ensure a differential binding of the transition state and reactant state, in line with Pauling's proposal[41] and as also proposed for other decarboxylase systems[42–44]. Inasmuch the here-uncovered catalytic principles are general features of enzyme catalysis remains to be seen in future studies.

Methods

Expression and purification of human OMPDC wild type. For expression of the human orotidine 5′-monophosphate decarboxylase domain (residues 224–480 of UMP synthase, UNIPROT P11172), we used a plasmid that contained a His_6-GST fusion construct. The coding sequence was then amplified using the primers 5′-GGC GCC ATG GAA CTC AGC TTC GGT GCA CG-3′ and 5′-TCA AAC ACC AAG TCT ACT CAA ATA CG-3′ and introduced into the Champion pET SUMO Expression System (Invitrogen), as described before[45]. The three leading amino acids (Gly-Ala-Met) from the initial GST fusion construct were kept as this increases the crystallization propensity of the protein. The plasmid that contained the His_6-SUMO-GAM-HsOMPDC$_{224–480}$ expression construct was isolated and used for mutagenesis experiments and protein expression. For protein expression, the fusion construct was transformed into Solu-BL21 *Escherichia coli* cells and grown under selective conditions (50 μg ml^{-1} kanamycin) in LB (lysogeny broth) medium. Main cultures (1 l) were prepared in the ZYM-5052 auto-induction medium and grown at 30 °C for 48 h and 180 revolutions per min (r.p.m.)[46]. The bacteria were harvested by centrifugation, shock-frozen in liquid nitrogen and stored at −80 °C until usage.

For protein purification, 10 g of cells (resulting from the expression of 1 l of bacterial culture) were resuspended in lysis buffer (50 mM Tris/HCl, 100 mM NaCl, 20 mM imidazole, pH 7.5) supplemented with 5 μg ml^{-1} DNaseI and phenylmethylsulfonyl fluoride (final concentration 1 mM), and subsequently lysed using a fluidizer (Microfluidics) operating at 15,000 p.s.i. (103,500 kPa). The cell lysate was clarified by centrifugation and the His_6-fusion protein was enriched using affinity chromatography (Ni-NTA FF 16/10, GE Healthcare). The column was extensively washed with buffer that contained 76 mM imidazole before the protein was eluted with buffer that contained 300 mM imidazole. To cleave the SUMO (small ubiquitin-like modifier) fusion protein, the imidazole buffer was exchanged for the same buffer but devoid of imidazole using a desalting column (HiPrep 26/10, GE Healthcare). SUMO protease was added in a 8,000:1 molar ratio to the SUMO–OMPDC fusion protein and incubated at 6 °C for 60 min under gentle shaking. Cleaved SUMO protein and SUMO protease (both His-tagged) were removed using affinity chromatography (Ni-NTA FF 16/10, GE Healthcare). The flow-through that contained OMPDC was collected, concentrated by ultrafiltration and applied onto a S75 gel filtration column (HiLoad 16/60 Superdex 75, GE Healthcare) previously equilibrated with 20 mM HEPES/NaOH, pH 7.4. The protein concentration was determined spectrophotometrically using a calculated molar extinction coefficient of $\varepsilon_{280} = 18{,}450\ M^{-1}\ cm^{-1}$ (ref. [47]). OMPDC was concentrated to ~20 mg ml^{-1} and directly used for kinetic and structural studies. For storage at −80 °C, the protein was supplemented with 25% (w/v) glycerol.

Variant Asp312Asn was generated by site-directed mutagenesis using the following primers:

- foreword: 5′-GATATTTGAAAACCGGAAGTTTG-3′ and
- reverse: 5′-AAGAACTCATGGCATTTTG-3′.

Protein expression and purification were carried out as detailed for the wild-type protein.

Expression and purification of hsOMPDC variant Lys314AcLys. To substitute the catalytic residue Lys314 with acetyllysine, the plasmid that contained the His_6-SUMO-hsOMPDC expression construct was first amplified using the primers

- 5′-CTTGATATTTGAAGACCGGTAGTTTGCAGATATAGGAAACACAG-3′ and
- 5′-CTGTGTTTCCTATATCTGCAAACTACCGGTCTTCAAATATCAAG-3′.

according to the QuickChange protocol. The base triplet coding for Lys314 was changed to the TAG–amber codon sequence to incorporate acetyllysine at this position using the amber suppression system. The thus-generated plasmid was transformed into BL21(DE3)* *E. coli* cells along with pCDF-AcKRS3/PylT, which encodes an acetyllysyl–tRNA synthetase/$tRNA_{CUA}$ pair[48]. Cells were grown under selective conditions (50 μg ml^{-1} kanamycin and 75 μg ml^{-1} spectinomycin) overnight at 37 °C on a plate. LB medium (1 l) was inoculated with a bacterial preculture of a grown colony and cultivated at 37 °C to an optical density of 0.6 at 600 nm. Nicotinamide was added to a f.c. of 50 mM and the cultures were incubated for another 30 min. To induce protein expression, isopropyl-β-D-thiogalactoside and acetyllysine were added to a f.c. of 1 and 10 mM, respectively. The cultures were incubated at 30 °C for 24 h. After expression, bacteria were harvested by centrifugation, shock-frozen in liquid nitrogen and stored at −80 °C until usage. Protein purification was carried out using the same protocol as detailed for the wild-type protein. The relative yield of OMPDC with acetyllysine at position 314 amounted to 0.46 mg protein per g cells, that is, ~10% relative to that of the wild-type protein.

Spectrophotometric steady-state kinetic analysis of OMP turnover. To kinetically analyse the OMPDC-catalysed OMP decarboxylation under steady-state turnover conditions, we used a continuous spectrophotometric assay. The reactions were prepared in 20 mM HEPES/NaOH, pH 7.4, with varying concentrations of substrate OMP. The reaction progress was monitored by the change in absorbance at 285 nm, which results from the different molar extinction coefficients of substrate OMP and product UMP ($\Delta\varepsilon_{285}^{OMP–UMP} = 1{,}650\ M^{-1}\ cm^{-1}$). All the reactions were performed at 25 °C for 300 s. The absorbance changes were measured using a spectrophotometer (Jasco V-650) and a quartz cuvette with reduced volume (Hellma Analytics, QS, 10 mm, 200 μl). In the case of the wild-type protein, a final concentration of 0.15 μmol of enzyme was used. The reaction was started by adding enzyme to the substrate solution in a 1:10 ratio. For variant Lys314AcLys, the enzyme concentration was 7.6 μmol. The obtained data points were fitted according to the Michaelis–Menten and Hill equations.

ITC measurements for the steady-state kinetic analysis of OMP turnover and UMP binding. All the measurements were performed with a PEAK-ITC instrument (Malvern Panalytical) in 20 mM HEPES/NaOH, pH 7.4 at 25 °C and 750 r.p.m. stirring. OMP trisodium and UMP disodium salts were purchased from Sigma Aldrich (>99% purity). The protein concentration was determined photometrically at 280 nm using an ε_{280} of 18,450 $M^{-1}\ cm^{-1}$. Steady-state kinetic analysis of OMP decarboxylation by OMPDC was determined following a single injection of protein (20 μM in syringe, 10 μl injection volume, 210 μl cell volume) into 1 mM substrate solution (0.95 μM protein after injection). The heat compensation was recorded for 2,700 s until reaction completion[49]. A second injection of enzyme was used to ascertain the complete substrate turnover. The raw data of a triplicate measurement were analysed using Microsoft Excel. The substrate-dependent decarboxylation rates were fitted in SigmaPlot 12.5 according to the Michaelis–Menten equation and Hill equation.

To determine the dissociation constant of OMPDC for the product UMP, the latter was titrated into a solution that contained 100 μM human OMPDC (dimer concentration) in the reaction cell in 19 subsequent injections steps of 2 μl each. To account for the differences in the dissociation constants of the two monomers of the homodimer, we applied different UMP concentrations (1, 2 and 5 mM). All the binding experiments were carried out as triplicates. The raw-data files were integrated using NitPic version 1.2.7[50] and fitted globally using Sedphat version 14.0 with local protein concentration correction factors[51,52]. For analysis of the binding of the product UMP and substrate OMP to the OMPDC variant Asp312Asn, the following concentrations and parameters were used:

- UMP binding: 202 μM OMPDC variant Asp312Asn, 2 mM UMP, buffer (HEPES 0.02 M, pH 7.4); reference power ITC, 8 μcal s^{-1}; stirring speed, 750 r.p.m.; cell temperature, 25 °C; 19 injections of 2 μl of UMP; spacing, 120 s.
- OMP binding: 176 μM OMPDC variant Asp312Asn, 2 mM OMP, buffer (HEPES 0.02 M, pH 7.4); reference power ITC, 8 μcal s^{-1}; stirring speed, 750 r.p.m.; cell temperature, 25 °C; 19 injections of 2 μl of OMP; spacing, 120 s.

Data visualization of a representative titration experiment was done using the analysis software supplied by the instrument's manufacturer.

Crystallization of OMPDC. Crystals of OMPDC were grown at 20 °C using the hanging-drop vapour diffusion method with VDXm crystallization plates (Hampton Research) as detailed before[45]. For crystal growth, the protein was diluted to 5 mg ml^{-1} in 20 mM HEPES/NaOH, pH 7.4. To obtain crystals of the resting-state enzyme, the reservoir solution was composed of 100 mM Tris/HCl pH 8.0, 1.8–2 M $(NH_4)_2SO_4$, 10 mM glutathione pH 8.0 and 5% (v/v) glycerol. The reservoir solution (400 µl) was applied into each well of the crystallization plate and 2 µl of the protein solution was mixed with the reservoir solution in a 1:1 ratio on a siliconized glass cover slide (Jena Analytics). Crystals appeared after ~3 days with a size of 100–200 µm and were either used for data collection or soaked with substrate analogues and transition-state analogues. Crystal-containing drops were supplemented with 2 µl of stabilization buffer (100 mM Tris/HCl pH 8.0, 2 M $(NH_4)_2SO_4$, 10 mM glutathione pH 8.0, 5% (v/v) glycerol and 1 M L-proline)[53]. The substrate analogues 6-carboxamido-UMP and 6-thiocarboxamido-UMP and the transition state analogue 6-aza-UMP were dissolved in cryoprotection buffer that contained 100 mM Tris/HCl pH 8.0, 2 M $(NH_4)_2SO_4$, 10 mM glutathione pH 8.0, 5% (v/v) glycerol, 1 M and L-proline, and diluted to a final concentration of 12.5 mM. OMPDC crystals were soaked in four subsequent steps of 30 min each with linearly increasing ligand concentrations. The crystals were then fished, flash–cooled in liquid nitrogen and stored until data collection.

For crystallization of the UMP product complex, OMPDC was mixed with UMP dissolved in 20 mM Na/HEPES pH 7.4 to obtain a f.c. of 25 mM and then incubated for 15 min at 20 °C. The protein solution (2 µl) was supplemented with reservoir solution (100 mM Tris/HCl pH 7.8, 1.6–1.8 M $(NH_4)_2SO_4$, 10 mM freshly prepared glutathione) in a 1:1 ratio. Crystals appeared after ~3 days with a size of 100–200 µm. To allow further crystal growth, the crystallization plates were incubated for another 10 days at 20 °C. The crystal-containing droplets were supplemented with 2 µl of stabilization solution (100 mM Tris/HCl pH 7.8, 1.8 M $(NH_4)_2SO_4$, 25 mM UMP, 10 mM freshly prepared glutathione) before the crystals were directly transferred into cryoprotection solution (100 mM Tris/HCl pH 7.8, 1.8 M $(NH_4)_2SO_4$, 25 mM UMP, 10 mM freshly prepared glutathione, 20% (v/v) glycerol). To crystallize the protein in a complex with the transition-state analogue BMP, human OMPDC was mixed with BMP previously dissolved in 20 mM Na/HEPES pH 7.4 to a f.c. of 10 mM and incubated for 15 min at 20 °C. The crystallization set-up, post-crystallization treatment and cryoprotection were identical to the aforementioned protocol for the OMPDC:UMP complex.

To grow crystals of OMPDC variant Lys314AcLys in the resting state, a reservoir solution with a slightly increased ammonium sulfate concentration was used (100 mM Tris/HCl pH 8.0, 1.9–2.1 M $(NH_4)_2SO_4$, 10 mM freshly prepared glutathione, 5% (v/v) glycerol). The formation of the crystals occurred over similar timescales to those observed for the wild-type protein. Crystals with a size of ~100–200 µm were transferred into cryoprotection solution (100 mM Tris/HCl pH 8.0, 2.0 M $(NH_4)_2SO_4$, 10 mM freshly prepared glutathione, 5% (v/v) glycerol, 1 M L-proline) and incubated for 5 min. Crystals were then fished and flash-cooled in liquid nitrogen. For the substrate soaking experiments with crystals of OMPDC variant Lys314AcLys, the crystals were prepared as described above and soaked with an OMP solution (50 mM OMP in 100 mM Tris/HCl pH 8.0 supplemented with 2.0 M $(NH_4)_2SO_4$, 10 mM freshly prepared glutathione, 5% (v/v) glycerol) for a duration of 1–30 min. Crystals were then fished and flash-cooled in liquid nitrogen.

X-ray data collection, processing and model building. Diffraction data of single OMPDC crystals were collected using synchrotron radiation at beamlines P14 and P13 of DESY/EMBL at wavelengths, as detailed in Supplementary Table 1. Data were collected at a cryogenic temperature of 100 K using either an EIGER 16M or PILATUS 6M detector, respectively. To minimize the radiation-induced damage of protein crystals, the radiation dose was determined before each measurement and the total radiation dose adjusted to 1 MGy. Protein crystals of variant Lys314AcLys in complex with substrate OMP were exposed to a total dose of 0.5 MGy to prevent radiation-induced decarboxylation of the enzyme-bound substrate. Diffraction data analysis, integration, correction, scaling, postrefinement and space-group assignment were carried out with the XDS program suite[54]. In the case of datasets collected for substrate-soaked crystals, data were further processed with the STARANISO server (http://staraniso.globalphasing.org, Global Phasing Limited)[55]. For subsequent iterative refinement cycles and model building, we employed REFMAC[56], PHENIX.REFINE[57], SHELX[58] and COOT[59], which yielded almost identical structural models with a comparable quality to that of the electron density maps. Ligands were refined with either relaxed (REFMAC and PHENIX.REFINE) or no restraints (SHELX). For phasing, Protein Data Bank (PDB) entries 2QCD and 2QCE were used for datasets refined to space groups $C222_1$ and $P2_1$, respectively. The geometry of the structure was validated using MolProbity[60]. Representations of structures were prepared using PyMOL[61]. The Ramachandran statistics are detailed in Supplementary Table 1.

Quantum chemical calculations of the MEPs. The substrate OMP was truncated to include only the orotic acid moiety (the N1 bond to the ribose ring was cut and saturated with a hydrogen atom). The resulting structure was optimized with different structural variations to generate the original substrate (protonated), carbanion transition state and the product state. The level of theory used was B3LYP[62–64] with use of the D3 empirical correction proposed by Grimme et al.[65] with Becke–Johnson (BJ) damping[66]. The basis set applied was def2-SVP[67] and the calculation was carried out with the integral equation formalism polarizable continuum model[68], with water as the solvent. The reason for this choice was the high polarity of the active site. However, we found that the results were not strongly affected by this choice. All the calculations were carried out with the Gaussian16 RevA.03 program package[69].

Dihedral potential scans. Using the same model as that applied for the calculation of the MEPs, the structures were reoptimized at the same level of theory with the ORCA 4.0.1 program package[70], applying resolution of the identity approximations with the default auxiliary basis set[71]. Note that the functional form is different for the B3LYP model between the program packages. Both the protonated and deprotonated forms of the model reactant were used for constrained optimizations. Although the profile is given as a function of the dihedral C4–C5–C6–C7, the profile was more stable with the use of C2–N1–C6–C7, which avoids spurious bends of the orotic acid ring. Increments of 5° were used at each step and the results were then analysed for the default dihedral angle.

DFT QM/MM optimizations. Structure optimizations to determine the origin of the carboxylate moiety kink (Supplementary Fig. 2) were performed by making use of the crystal structure and interfacing ORCA 4.0.1 and AMBER18[72] with the CHEMSHELL 3.5.0[73] QM/MM software. The orotic acid ring was included in the QM region, cutting the bond between N1 and the ribose ring, and saturating the dangling bond with a link hydrogen atom according to the standard procedure in CHEMSHELL[73]. All atoms in the system, except in the QM region, were kept frozen.

The MM force field for the substrate was prepared with AMBER18, using ff14SB[74] and GAFF[75,76]. The acetylated Lys314 (AcK) was kept for these calculations, which were parametrized by adding the hydrogen atoms and optimizing them with Gaussian16. The optimization was performed at the B3LYP/def2-SVP level with the D3(BJ) correction. This optimized structure was employed to fit the restrained electrostatic potential charges[77] at the HF/6-31G* level, following the standard procedure. AMBER atom types were assigned to this residue. In the same fashion, the force-field parameters were generated for the substrate OMP, but with the GAFF atom types in this case.

Potential of mean force umbrella sampling calculations. The dynamics were performed employing AMBER18 with ff14SB and GAFF. The acetylated Lys314 from the crystal structure data was restored to a regular lysine residue to study the catalysed reaction in the wild-type context. The substrate parameters employed for the QM/MM phase were also used in these dynamics. The system was solvated in a periodic box, which extended 8 Å away from the protein, and neutralized with Na^+ counterions. All the Arg, Lys, Asp and Glu residues were charged. The histidines were set as HID283, HID393, HIE237, HIE305, HIE343, HIE414 and HIP362.

A cutoff of 8 Å was employed for the non-bonded interactions, using particle-mesh Ewald summation with a fourth-order B-spline interpolation and a tolerance of 10^{-5}. The non-bonded list was updated every 50 fs and the time step was set to 1 fs. The system was first minimized for 5,000 cycles, 2,000 with the steepest descent and 3,000 with a conjugate gradient, restraining all the non-hydrogen atoms to their Cartesian coordinates with a force constant of 10 kcal mol^{-1} Å^{-2}. We then minimized the system for another 5,000 cycles, 2,000 with the steepest descent and 3,000 with a conjugate gradient, restraining the backbone heavy atoms to their Cartesian coordinates with a force constant of 10 kcal mol^{-1} Å^{-2}. All the molecular mechanics molecular dynamics results (Supplementary Fig. 4) were obtained by carrying out production runs from this setup.

The QM/MM molecular dynamics simulations were carried out with the DFTB3 semiempirical Hamiltonian[78]. The QM region was defined by the orotidine ring, and the side chains of D312, D317, K314 and K281, which included the carboxylic and the amine moiety, were truncated at the following C atom. The reaction coordinate was defined by the C–C bond that was cleaved, and we employed a restraint of 350.0 kcal mol^{-2} for each window of the PMF. We started with 1.50, 1.80, 2.10, 2.40, 2.70, 3.00, 3.30, 3.60 and 3.90 Å distances, and minimized the system for 5,000 cycles, 2,000 with the steepest descent and 3,000 with a conjugate gradient. We then heated the system for 200 ps, from 0 to 300 K, slowly increasing the temperature at equal intervals using the NVT ensemble and Langevin dynamics with a collision frequency of 2.0 ps^{-1}. We then equilibrated the system for another 200 ps in the NPT ensemble at 300 K with isotropic position scaling and a relaxation time of 1.0 ps. The production phase was then performed at the same ensemble, with the same parameters for 2 ns. The weighted histogram analysis method[79] was then applied to obtain the potential of the mean force (Fig. 2d).

The last structure from the performed windows was used as the starting point for the following ones, incrementing the C–C distance by 0.05 Å. We first minimized the system for 5,000 cycles, 2,000 with the steepest descent and 3,000 with a conjugate gradient. Each window was then equilibrated for another 200 ps in the NPT ensemble at 300 K and with isotropic position scaling and a relaxation time of 1.0 ps. The production phases were performed at the same ensemble, with the same parameters as those for 2 ns.

Synthesis of substrate, substrate analogues and transition-state analogues. The protocols for the chemical synthesis of the substrate, substrate analogues and transition-state analogues are provided in the Supplementary Methods.

Reporting Summary. Further information on research design is available in the Nature Research Reporting Summary linked to this article.

Data availability

The refined structural protein models and corresponding structure-factor amplitudes are deposited under PDB accession codes 7OUZ (wild-type, BMP, crystal 1), 7OTU (wild-type, BMP, crystal 2), 6ZWY (wild-type, UMP, crystal 1), 7ASQ (wild-type, UMP, crystal 2), 6ZX1 (wild-type, aza-UMP), 7OV0 (wild-type, resting state), 6ZX2 (carboxamido-UMP), 6ZX3 (thiocarboxamido-UMP), 6ZWZ (variant K314AcK, resting state), 6YWU (variant K314AcK, UMP), 6YVK (variant K314AcK, 2 min soaking with OMP, 0.71 MGy dose), 6YVL (variant K314AcK, 2 min soaking with OMP, 1.42 MGy dose), 6YVM (variant K314AcK, 2 min soaking with OMP, 2.13 MGy dose), 6YVN (variant K314AcK, 2 min soaking with OMP, 2.84 MGy dose), 6YVO (variant K314AcK, 2 min soaking with OMP, 3.55 MGy dose), 6YWT (variant K314AcK, BMP), 7OQF (variant K314AcK, 5 min soaking with OMP), 7OQI (variant K314AcK, 10 min soaking with OMP), 7OQK (variant K314AcK, 15 min soaking with OMP), 7OQM (variant K314AcK, 20 min soaking with OMP), 7OQN (variant K314AcK, 30 min soaking with OMP), 7AM9 (variant K314AcK, 2 min soaking with OMP, merged dataset), 6ZX0 (variant K314AcK, OMP), 7Q1H (variant D312N, 2 min soaking with OMP) (Supplementary Table 1). The results of the quantum chemical calculations have been deposited in the GRO.data repository at https://doi.org/10.25625/6OOHE5. All other data are available on request.

Received: 23 July 2021; Accepted: 10 March 2022;
Published online: 21 April 2022

References

1. Radzicka, A. & Wolfenden, R. A proficient enzyme. *Science* **267**, 90–93 (1995).
2. Lee, J. K. & Houk, K. N. A proficient enzyme revisited: the predicted mechanism for orotidine monophosphate decarboxylase. *Science* **276**, 942–945 (1997).
3. Miller, B. G. & Wolfenden, R. Catalytic proficiency: the unusual case of OMP decarboxylase. *Annu. Rev. Biochem.* **71**, 847–885 (2002).
4. Richard, J. P., Amyes, T. L. & Reyes, A. C. Orotidine 5′-monophosphate decarboxylase: probing the limits of the possible for enzyme catalysis. *Acc. Chem. Res.* **51**, 960–969 (2018).
5. Wu, N., Mo, Y., Gao, J. & Pai, E. F. Electrostatic stress in catalysis: structure and mechanism of the enzyme orotidine monophosphate decarboxylase. *Proc. Natl Acad. Sci. USA* **97**, 2017–2022 (2000).
6. Appleby, T. C., Kinsland, C., Begley, T. P. & Ealick, S. E. The crystal structure and mechanism of orotidine 5′-monophosphate decarboxylase. *Proc. Natl Acad. Sci. USA* **97**, 2005–2010 (2000).
7. Miller, B. G., Hassell, A. M., Wolfenden, R., Milburn, M. V. & Short, S. A. Anatomy of a proficient enzyme: the structure of orotidine 5′-monophosphate decarboxylase in the presence and absence of a potential transition state analog. *Proc. Natl Acad. Sci. USA* **97**, 2011–2016 (2000).
8. Harris, P., Navarro Poulsen, J. C., Jensen, K. F. & Larsen, S. Structural basis for the catalytic mechanism of a proficient enzyme: orotidine 5′-monophosphate decarboxylase. *Biochemistry* **39**, 4217–4224 (2000).
9. Amyes, T. L., Wood, B. M., Chan, K., Gerlt, J. A. & Richard, J. P. Formation and stability of a vinyl carbanion at the active site of orotidine 5′-monophosphate decarboxylase: pK_a of the C-6 proton of enzyme-bound UMP. *J. Am. Chem. Soc.* **130**, 1574–1575 (2008).
10. Chan, K. K. et al. Mechanism of the orotidine 5′-monophosphate decarboxylase-catalyzed reaction: evidence for substrate destabilization. *Biochemistry* **48**, 5518–5531 (2009).
11. Jencks, W. P. Binding energy, specificity, and enzymic catalysis: the Circe effect. *Adv. Enzymol. Relat. Areas Mol. Biol.* **43**, 219–410 (1975).
12. Warshel, A. & Florián, J. Computer simulations of enzyme catalysis: finding out what has been optimized by evolution. *Proc. Natl.# Acad. Sci. USA* **95**, 5950–5955 (1998).
13. Warshel, A., Štrajbl, M., Villa, J. & Florián, J. Remarkable rate enhancement of orotidine 5′-monophosphate decarboxylase is due to transition-state stabilization rather than to ground-state destabilization. *Biochemistry* **39**, 14728–14738 (2000).
14. Warshel, A., Florián, J., Štrajbl, M. & Villà, J. Circe effect versus enzyme preorganization: what can be learned from the structure of the most proficient enzyme? *ChemBioChem* **2**, 109–111 (2001).
15. Goryanova, B., Amyes, T. L. & Richard, J. P. Role of the carboxylate in enzyme-catalyzed decarboxylation of orotidine 5′-monophosphate: transition state stabilization dominates over ground state destabilization. *J. Am. Chem. Soc.* **141**, 13468–13478 (2019).
16. Wu, N., Gillon, W. & Pai, E. F. Mapping the active site–ligand interactions of orotidine 5′-monophosphate decarboxylase by crystallography. *Biochemistry* **41**, 4002–4011 (2002).
17. Wittmann, J. G. et al. Structures of the human orotidine-5′-monophosphate decarboxylase support a covalent mechanism and provide a framework for drug design. *Structure* **16**, 82–92 (2008).
18. Neumann, P. & Tittmann, K. Marvels of enzyme catalysis at true atomic resolution: distortions, bond elongations, hidden flips, protonation states and atom identities. *Curr. Opin. Struct. Biol.* **29**, 122–133 (2014).
19. Noren, C. J., Anthony-Cahill, S. J., Griffith, M. C. & Schultz, P. G. A general method for site-specific incorporation of unnatural amino acids into proteins. *Science* **244**, 182–188 (1989).
20. Takusagawa, F. & Shimada, A. The crystal structure of orotic acid monohydrate (vitamin B13). *Bull. Chem. Soc. Jpn* **46**, 2011–2019 (1973).
21. Lüdtke, S. et al. Sub-ångström-resolution crystallography reveals physical distortions that enhance reactivity of a covalent enzymatic intermediate. *Nat. Chem.* **5**, 762–767 (2013).
22. Asztalos, P. et al. Strain and near attack conformers in enzymic thiamin catalysis: X-ray crystallographic snapshots of bacterial transketolase in covalent complex with donor ketoses xylulose 5-phosphate and fructose 6-phosphate, and in noncovalent complex with acceptor aldose ribose 5-phosphate. *Biochemistry* **46**, 12037–12052 (2007).
23. Gurusaran, M., Shankar, M., Nagarajan, R., Helliwell, J. R. & Sekar, K. Do we see what we should see? Describing non-covalent interactions in protein structures including precision. *IUCrJ* **1**, 74–81 (2014).
24. Owen, R. L., Rudiño-Piñera, E. & Garman, E. F. Experimental determination of the radiation dose limit for cryocooled protein crystals. *Proc. Natl Acad. Sci. USA* **103**, 4912–4917 (2006).
25. Frank, R. A., Titman, C. M., Pratap, J. V., Luisi, B. F. & Perham, R. N. A molecular switch and proton wire synchronize the active sites in thiamine enzymes. *Science* **306**, 872–876 (2004).
26. Dai, S. et al. Low-barrier hydrogen bonds in enzyme cooperativity. *Nature* **573**, 609–613 (2019).
27. Rabe von Pappenheim, F. et al. Structural basis for antibiotic action of the B1 antivitamin 2′-methoxy-thiamine. *Nat. Chem. Biol.* **16**, 1237–1245 (2020).
28. Kluger, R. Decarboxylation, CO_2 and the reversion problem. *Acc. Chem. Res.* **48**, 2843–2849 (2015).
29. Kong, D., Moon, P. J., Lui, E. K., Bsharat, O. & Lundgren, R. J. Direct reversible decarboxylation from stable organic acids in dimethylformamide solution. *Science* **369**, 557–561 (2020).
30. Desai, B. J. et al. Investigating the role of a backbone to substrate hydrogen bond in OMP decarboxylase using a site-specific amide to ester substitution. *Proc. Natl Acad. Sci. USA* **111**, 15066–15071 (2014).
31. Jencks, W. P. When is an intermediate not an intermediate? Enforced mechanisms of general acid–base, catalyzed, carbocation, carbanion, and ligand exchange reaction. *Acc. Chem. Res.* **13**, 161–169 (1980).
32. Schwander, T., von Borzyskowski, L. S., Burgener, S., Cortina, N. S. & Erb, T. J. A synthetic pathway for the fixation of carbon dioxide in vitro. *Science* **354**, 900–904 (2016).
33. Stoffel, G. M. et al. Four amino acids define the CO_2 binding pocket of enoyl-CoA carboxylases/reductases. *Proc. Natl Acad. Sci. USA* **116**, 13964–13969 (2019).
34. Whitney, S. M., Houtz, R. L. & Alonso, H. Advancing our understanding and capacity to engineer nature's CO_2-sequestering enzyme, Rubisco. *Plant Phys.* **155**, 27–35 (2011).
35. Zhou, S., Nguyen, B. T., Richard, J. P., Kluger, R. & Gao, J. Origin of free energy barriers of decarboxylation and the reverse process of CO_2 capture in dimethylformamide and in water. *J. Am. Chem. Soc.* **143**, 137–141 (2021).
36. Ho, M. C., Ménétret, J. F., Tsuruta, H. & Allen, K. N. The origin of the electrostatic perturbation in acetoacetate decarboxylase. *Nature* **459**, 393–397 (2009).
37. Fujihashi, M. et al. Substrate distortion contributes to the catalysis of orotidine 5′-monophosphate decarboxylase. *J. Am. Chem. Soc.* **135**, 17432–17443 (2013).
38. Warshel, A. et al. Electrostatic basis for enzyme catalysis. *Chem. Rev.* **106**, 3210–3235 (2006).
39. Warshel, A. Electrostatic origin of the catalytic power of enzymes and the role of preorganized active sites. *J. Biol. Chem.* **273**, 27035–27038 (1998).
40. Prah, A., Frančišković, E., Mavri, J. & Stare, J. Electrostatics as the driving force behind the catalytic function of the monoamine oxidase A enzyme confirmed by quantum computations. *ACS Catal.* **9**, 1231–1240 (2019).
41. Pauling, L. Nature of forces between large molecules of biological interest. *Nature* **161**, 707–709 (1948).
42. Wille, G. et al. The catalytic cycle of a thiamin diphosphate enzyme examined by cryocrystallography. *Nat. Chem. Biol.* **2**, 324–328 (2006).
43. Meyer, D. et al. Double duty for a conserved glutamate in pyruvate decarboxylase: evidence of the participation in stereoelectronically controlled decarboxylation and in protonation of the nascent carbanion/enamine intermediate. *Biochemistry* **49**, 8197–8212 (2010).

44. Kluger, R. & Tittmann, K. Thiamin diphosphate catalysis: enzymic and nonenzymic covalent intermediates. *Chem. Rev.* **108**, 1797–1833 (2008).
45. Wittmann, J. G. & Rudolph, M. G. Pseudo-merohedral twinning in monoclinic crystals of human orotidine-5′-monophosphate decarboxylase. *Acta Crystallogr. D* **63**, 744–749 (2007).
46. Studier, F. W. Protein production by auto-induction in high-density shaking cultures. *Prot. Expres Purif.* **41**, 207–234 (2005).
47. Gasteiger, E. et al. in *The Proteomics Protocols Handbook* (ed. Walker, J. M.) 571–607 (Springer, 2005).
48. Neumann, H., Peak-Chew, S. Y. & Chin, J. W. Genetically encoding Nε-acetyllysine in recombinant proteins. *Nat. Chem. Biol.* **4**, 232–234 (2008).
49. Poduch, E. et al. Design of inhibitors of orotidine monophosphate decarboxylase using bioisosteric replacement and determination of inhibition kinetics. *J. Med. Chem.* **49**, 4937–4945 (2006).
50. Keller, S. et al. High-precision isothermal titration calorimetry with automated peak-shape analysis. *Anal. Chem.* **84**, 5066–5073 (2012).
51. Houtman, J. C. et al. Studying multisite binary and ternary protein interactions by global analysis of isothermal titration calorimetry data in SEDPHAT: application to adaptor protein complexes in cell signaling. *Protein Sci.* **16**, 30–42 (2007).
52. Zhao, H., Piszczek, G. & Schuck, P. SEDPHAT—a platform for global ITC analysis and global multi-method analysis of molecular interactions. *Methods* **76**, 137–148 (2015).
53. Pemberton, T. A. et al. Proline: mother nature's cryoprotectant applied to protein crystallography. *Acta Crystallogr. D* **68**, 1010–1018 (2012).
54. Kabsch, W. XDS. *Acta Crystallogr. D* **66**, 125–132 (2010).
55. Vonrhein, C. et al. Advances in automated data analysis and processing within autoPROC, combined with improved characterisation, mitigation and visualisation of the anisotropy of diffraction limits using STARANISO. *Acta Crystallogr. A* **74**, a360 (2018).
56. Murshudov, G. N. et al. REFMAC5 for the refinement of macromolecular crystal structures. *Acta Crystallogr. D* **67**, 355–367 (2011).
57. Adams, P. D. et al. PHENIX: a comprehensive Python-based system for macromolecular structure solution. *Acta Crystallogr. D* **66**, 213–221 (2010).
58. Sheldrick, G. M. A short history of SHELX. *Acta Crystallogr. A* **64**, 112–122 (2008).
59. Emsley, P., Lohkamp, B., Scott, W. G. & Cowtan, K. Features and development of Coot. *Acta Crystallogr. D* **66**, 486–501 (2010).
60. Chen, V. B. et al. MolProbity: all-atom structure validation for macromolecular crystallography. *Acta Crystallogr. D* **66**, 12–21 (2010).
61. The PyMOL Molecular Graphics System v.2.0 (Schrödinger, LLC).
62. Vosko, S. H., Wilk, L. & Nusair, M. Accurate spin-dependent electron liquid correlation energies for local spin density calculations: a critical analysis. *Can. J. Phys.* **58**, 1200–1211 (1980).
63. Becke, A. D. Density-functional thermochemistry. III. The role of exact exchange. *J. Chem. Phys.* **98**, 5648–5652 (1993).
64. Lee, C., Yang, W. & Parr, R. G. Development of the Colle–Salvetti correlation-energy formula into a functional of the electron density. *Phys. Rev. B* **37**, 785–789 (1988).
65. Grimme, S., Antony, J., Ehrlich, S. & Krieg, H. A consistent and accurate ab initio parametrization of density functional dispersion correction (DFT-D) for the 94 elements H–Pu. *J. Chem. Phys.* **132**, 154104 (2010).
66. Grimme, S., Ehrlich, S. & Goerigk, L. Effect of the damping function in dispersion corrected density functional theory. *J. Comp. Chem.* **32**, 1456–1465 (2011).
67. Weigend, F. & Ahlrichs, R. Balanced basis sets of split valence, triple zeta valence and quadruple zeta valence quality for H to Rn: design and assessment of accuracy. *Phys. Chem. Chem. Phys.* **7**, 3297–3305 (2005).
68. Tomasi, J., Mennucci, B. & Cammi, R. Quantum mechanical continuum solvation models. *Chem. Rev.* **105**, 2999–3094 (2005).
69. Frisch, M. J. et al. Gaussian 16 Revision A.03 (Gaussian, Inc., 2016).
70. Neese, F. Software update: the ORCA program system, version 4.0. *WIREs Comp. Mol. Sci.* **8**, e1327 (2018).
71. Weigend, F. Accurate Coulomb-fitting basis sets for H to Rn. *Phys. Chem. Chem. Phys.* **8**, 1057–1065 (2006).
72. Case, D. et al. AMBER 18 (Univ. California, 2018).
73. Metz, S., Kästner, J., Sokol, A. A., Keal, T. W. & Sherwood, P. CHEMSHELL—a modular software package for QM/MM simulations. *WIREs Comp. Mol. Sci.* **4**, 101–110 (2014).
74. Maier, J. A. Improving the accuracy of protein side chain and backbone parameters from ff99SB. *J. Chem. Theory Comput.* **11**, 3696–3713 (2015).
75. Wang, J., Wang, W., Kollman, P. A. & Case, D. A. Automatic atom type and bond type perception in molecular mechanical calculations. *J. Mol. Graph. Model.* **25**, 247–260 (2006).
76. Wang, J., Wolf, R. M., Caldwell, J. W., Kollman, P. A. & Case, D. A. Development and testing of a general AMBER force field. *J. Comput. Chem.* **25**, 1157–1174 (2004).
77. Bayly, C. I., Cieplak, P., Cornell, W. & Kollman, P. A. A well-behaved electrostatic potential based method using charge restraints for deriving atomic charges: the RESP model. *J. Phys. Chem.* **97**, 10269–10280 (1993).
78. Gaus, M., Goez, A. & Elstner, M. Parametrization and benchmark of DFTB3 for organic molecules. *J. Chem. Theory Comput.* **9**, 338–354 (2013).
79. Grossfield, A. WHAM: the weighted histogram analysis method v.2.0.9. (University of Rochester Medical Center, accessed 15 November 2013); http://membrane.urmc.rochester.edu/?page_id=126

Acknowledgements

This study was supported by the Max-Planck Society and the DFG-funded Göttingen Graduate Center for Neurosciences, Biophysics, and Molecular Biosciences GGNB. We acknowledge access to beamline P14 at DESY/EMBL. We thank M. Rudolph for providing a plasmid for recombinant expression of human OMPDC and H. Neumann for providing the AMBER suppression system for the expression of acetyllysine residues. We thank J. Chin, G. Howe and A. Pearson for discussion. We thank G. Bricogne and his team from Global Phasing Limited for discussion regarding anisotropic data processing.

Author contributions

K.T., R.A.M. and U.D. designed and coordinated the project. S.R. expressed, purified, crystallized and enzymatically characterized proteins under the supervision of K.T. S.R. collected crystallographic datasets with support from A.C., G.B. and T.S. S.R. and F.R.v.P. refined the structures with support from A.C., G.B., T.S. and K.T. L.L.K. expressed, purified and crystallized variant Asp312Asn. S.R., F.R.v.P. and K.T. interpreted the crystallographic data. J.U. carried out the electronic structure calculations and molecular dynamics calculations. A.B. carried out molecular dynamics calculations under the supervision of J.U. J.U. and R.A.M. interpreted the calculations. M.K. and T.S. chemically synthesized the substrate and transition-state analogues under the supervision of U.D. S.R., J.U., R.K., U.D, R.A.M. and K.T. discussed the enzymatic reaction mechanism. S.R., J.U., T.S., R.A.M. and K.T. wrote the paper with input from all the other authors.

Competing interests

The authors declare no competing interests.

Additional information

Extended data is available for this paper at https://doi.org/10.1038/s41929-022-00771-w.

Supplementary information The online version contains supplementary material available at https://doi.org/10.1038/s41929-022-00771-w.

Correspondence and requests for materials should be addressed to Ricardo A. Mata or Kai Tittmann.

Peer review information *Nature Catalysis* thanks the anonymous reviewers for their contribution to the peer review of this work.

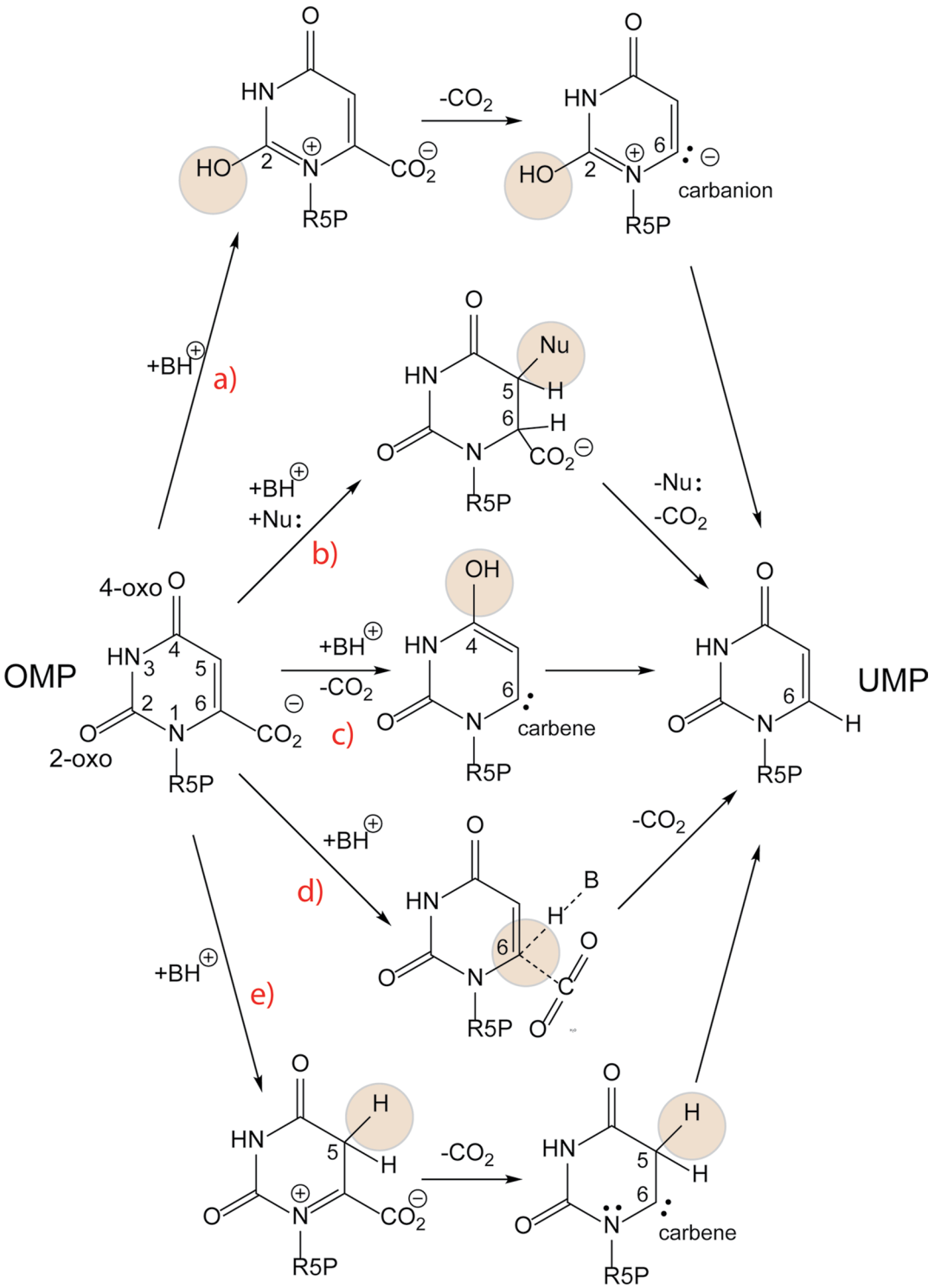

Extended Data Fig. 1 | Suggested mechanisms of OMPDC-catalysed decarboxylation of OMP. Suggested mechanisms of OMPDC-catalysed decarboxylation of OMP. (**a**) protonation at 2-oxo, (**b**) attack of a nucleophile at C5, (**c**) protonation at 4-oxo, (**d**) electrophilic displacement, (**e**) protonation at C5. Scheme adapted from[3]. The currently accepted mechanism invoking a combination of transition-state stabilisation and ground-state destabilisation is shown in Fig. 1a of the main manuscript. Abbreviations: OMPDC, orotidine-5′-monophosphate decarboxylase; OMP, orotidine-5′-monophosphate.

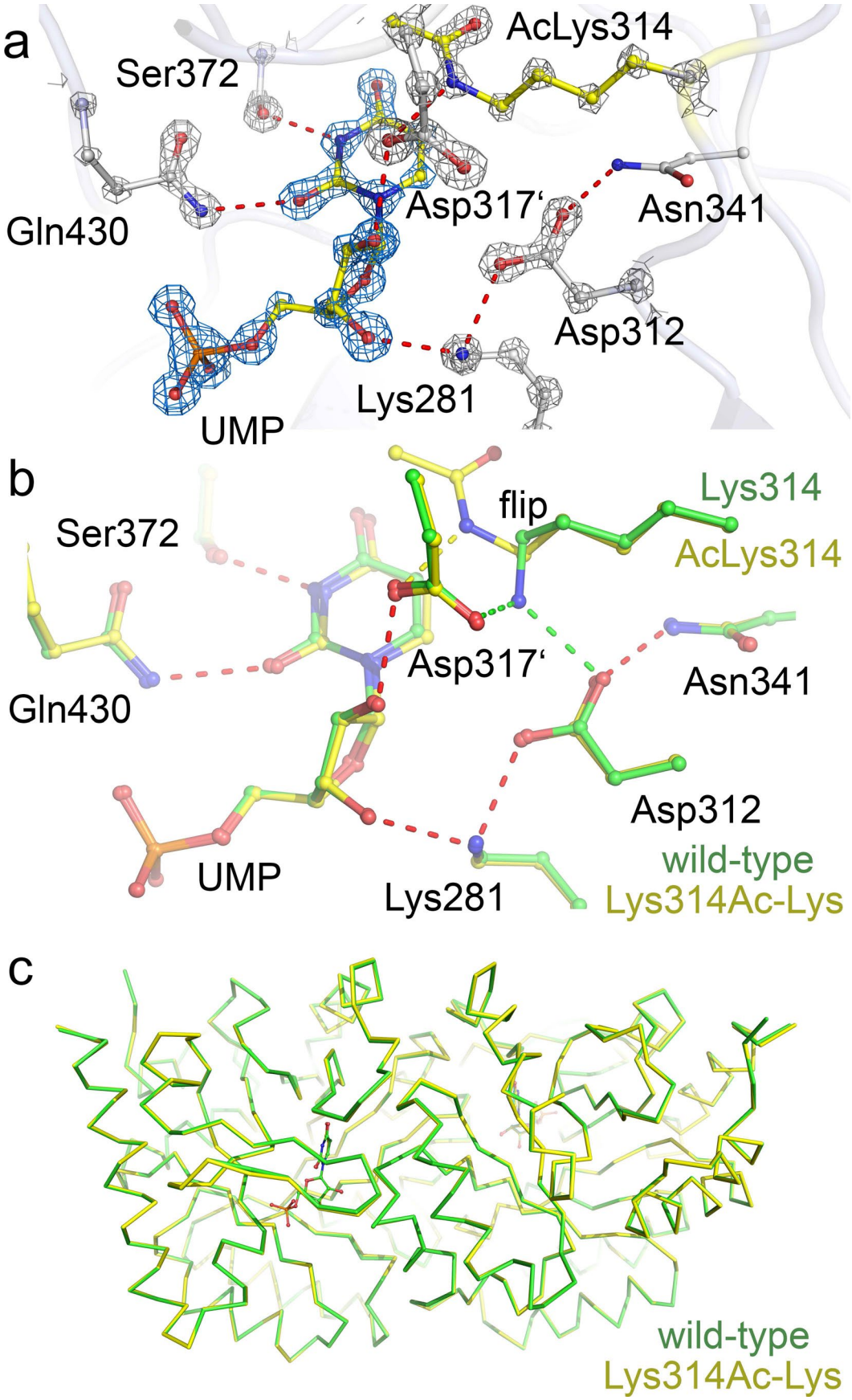

Extended Data Fig. 2 | See next page for caption.

Extended Data Fig. 2 | Structure of human OMPDC variant Lys314Ac-Lys in complex with product UMP at a resolution of 1.10 Å. Structure of human OMPDC variant Lys314Ac-Lys in complex with product UMP at a resolution of 1.10 Å. (**a**) Structure of the active site showing the bound product and interacting protein groups. UMP and mutated residue AcLys314 are highlighted in yellow color. The structural model is superposed with the corresponding 2mF-DFc electron density map at a contour level of 4σ (UMP: blue, protein residues: grey). H-bonding interactions are indicated. (**b**) Superposition of the active sites of human OMPDC wild-type in complex with UMP (green, this study) with variant Lys314AcLys (yellow). Shown are the bound product UMP and interacting protein groups. Note the conserved binding mode of the product and interactions with protein groups except for a flip of the Cδ-Cε bond of the Lys side-chain in the variant. (**c**) Superposition of the backbone of human OMPDC wild-type in complex with UMP (green, this study) with variant Lys314AcLys (yellow). The RMSD of the C_α carbons amounts to 0.15 Å. Crystallographic statistics are provided in Supplementary Table 1. Abbreviations: OMPDC, orotidine-5′-monophosphate decarboxylase; OMP, orotidine-5′-monophosphate; UMP, uridine-5′-monophosphate; RMSD, root mean square deviation.

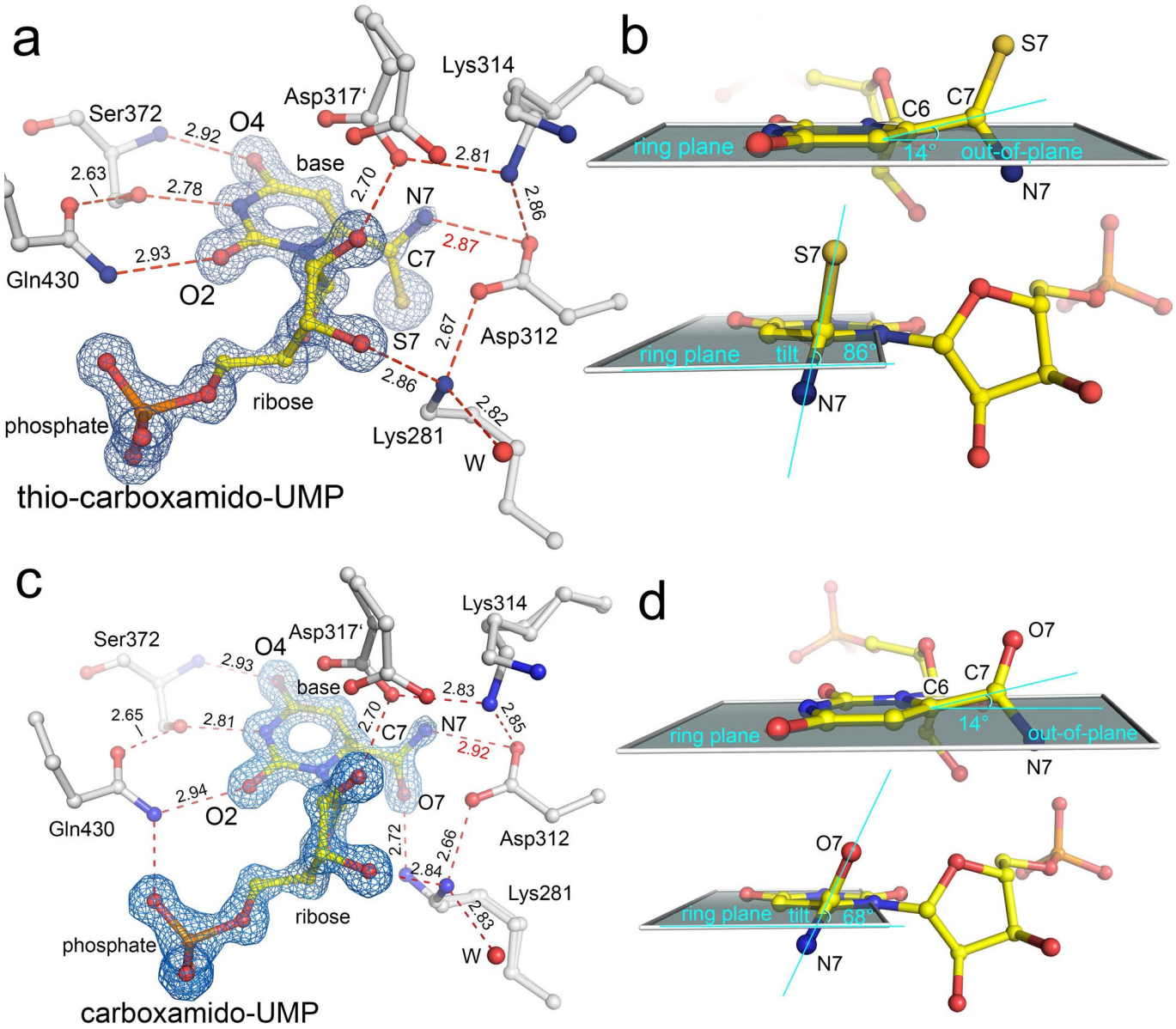

Extended Data Fig. 3 | Structures of human OMPDC wild-type in complex with substrate analogs. Structures of human OMPDC wild-type in complex with substrate analogs. (**a**) Structure of human OMPDC in complex with substrate analog 6-thio-carboxyamido-UMP showing the active site with the bound analog and interacting protein groups. The structural model of the analog is super-posed with the corresponding 2mFo-DFc electron density map at a contour level of 3.3σ. Hydrogen-bonding interactions are indicated. Note the H-bond interaction between the N7 atom of the analog with Asp312 similar to the genuine substrate (see Fig. 2a of the main manuscript). (**b**) Physical distortion of the C6-C7 bond of the analog relative to the base ring plane shown in grey and tilt of the thio-carboxamido plane relative to the base ring plane shown in grey. (**c**) Structure of human OMPDC in complex with substrate analog 6-carboxyamido-UMP showing the active site with the bound analog and interacting protein groups. The structural model of the analog is superposed with the corresponding 2mFo-DFc electron density map at a contour level of 3σ. Hydrogen-bonding interactions are indicated. Note the H-bond interaction between the N7 atom of the analog with Asp312 similar to the genuine substrate (see Fig. 2a of the main manuscript). (**d**) Physical distortion of the C6-C7 bond of the analog relative to the base ring plane shown in grey and tilt of the carboxamido plane relative to the base ring plane shown in grey. Crystallographic statistics are provided in Supplementary Table 1. Abbreviations: OMPDC, orotidine-5′-monophosphate decarboxylase.

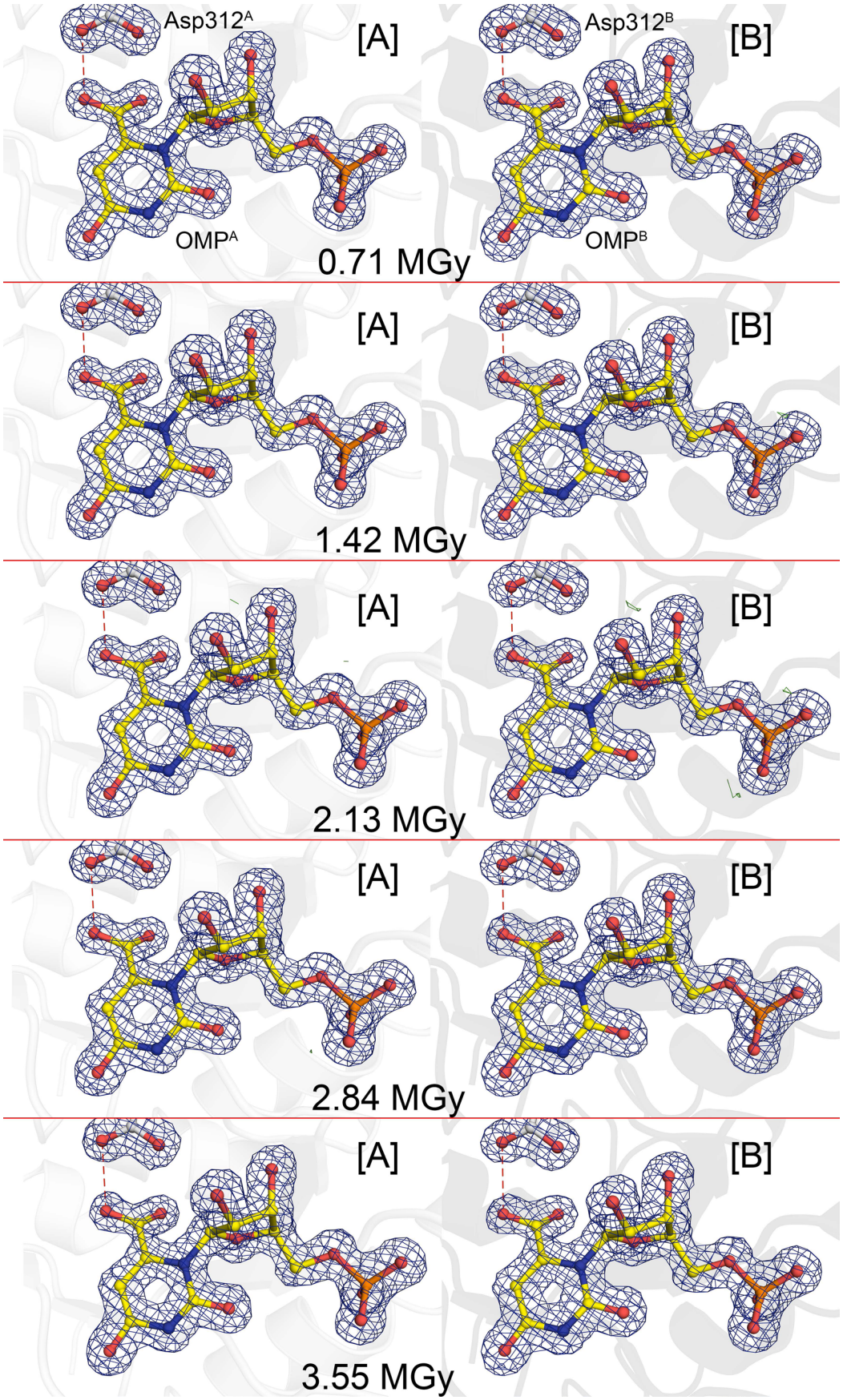

Extended Data Fig. 4 | See next page for caption.

Extended Data Fig. 4 | Dose-dependent structure analysis of human OMPDC in complex with substrate OMP. Dose-dependent structure analysis of human OMPDC in complex with substrate OMP. Datasets of crystals of OMPDC variant Lys31AcLys soaked with OMP for 2 min were collected at beamline P14 at DESY/EMBL Hamburg depositing calibrated doses as indicated. The refined structural models of bound substrate and interacting residue Asp312 are shown for both active sites of the homodimer. The structural models are superposed with the corresponding 2mFo-DFc electron density maps at a contour level of 1σ. No evidence for a radiation-induced decarboxylation of either the substrate or side chain of Asp312 was obtained. Refinements were carried out in space group $P2_1$ (containing a functional homodimer in the asymmetric unit) for all datasets. Crystallographic statistics are provided in Supplementary Table 1. Abbreviations: OMPDC, orotidine-5′-monophosphate decarboxylase; OMP, orotidine-5′-monophosphate.

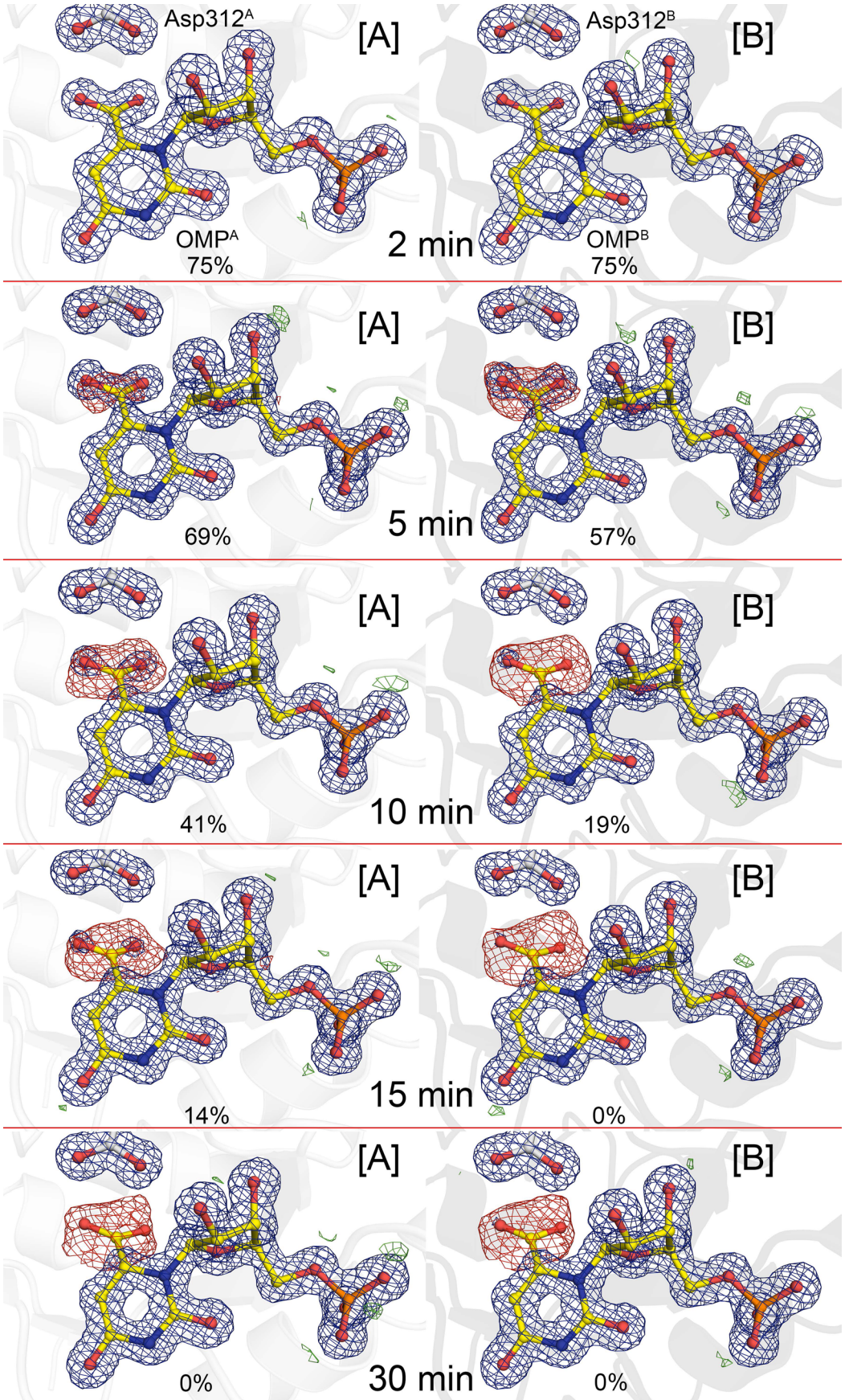

Extended Data Fig. 5 | See next page for caption.

Extended Data Fig. 5 | Time-resolved structural snapshots of OMPDC-catalysed conversion of substrate OMP into product UMP. Time-resolved structural snapshots of OMPDC-catalysed conversion of substrate OMP into product UMP. Crystals of human OMPDC variant Lys314AcLys were soaked with substrate OMP for different reaction times as indicated ranging from 2–30 min at 6 °C. The refined structural models of bound substrate and interacting residue Asp312 are shown for both active sites of the homodimer. The structural models are superposed with the corresponding 2mFo-DFc electron density maps at a contour level of 1σ (in blue). The refined occupancies of substrate OMP are shown. The difference electron density relative to the dataset obtained at 2 min is shown for all later datasets at a contour level of 3σ in red colour indicating the progressive decarboxylation of substrate OMP over time. Refinements were carried out in space group $P2_1$ (containing a functional homodimer in the asymmetric unit) for all datasets. Crystallographic statistics are provided in Supplementary Table 1. Abbreviations: OMPDC, orotidine-5′-monophosphate decarboxylase; OMP, orotidine-5′-monophosphate; UMP, uridine-5′-monophosphate.

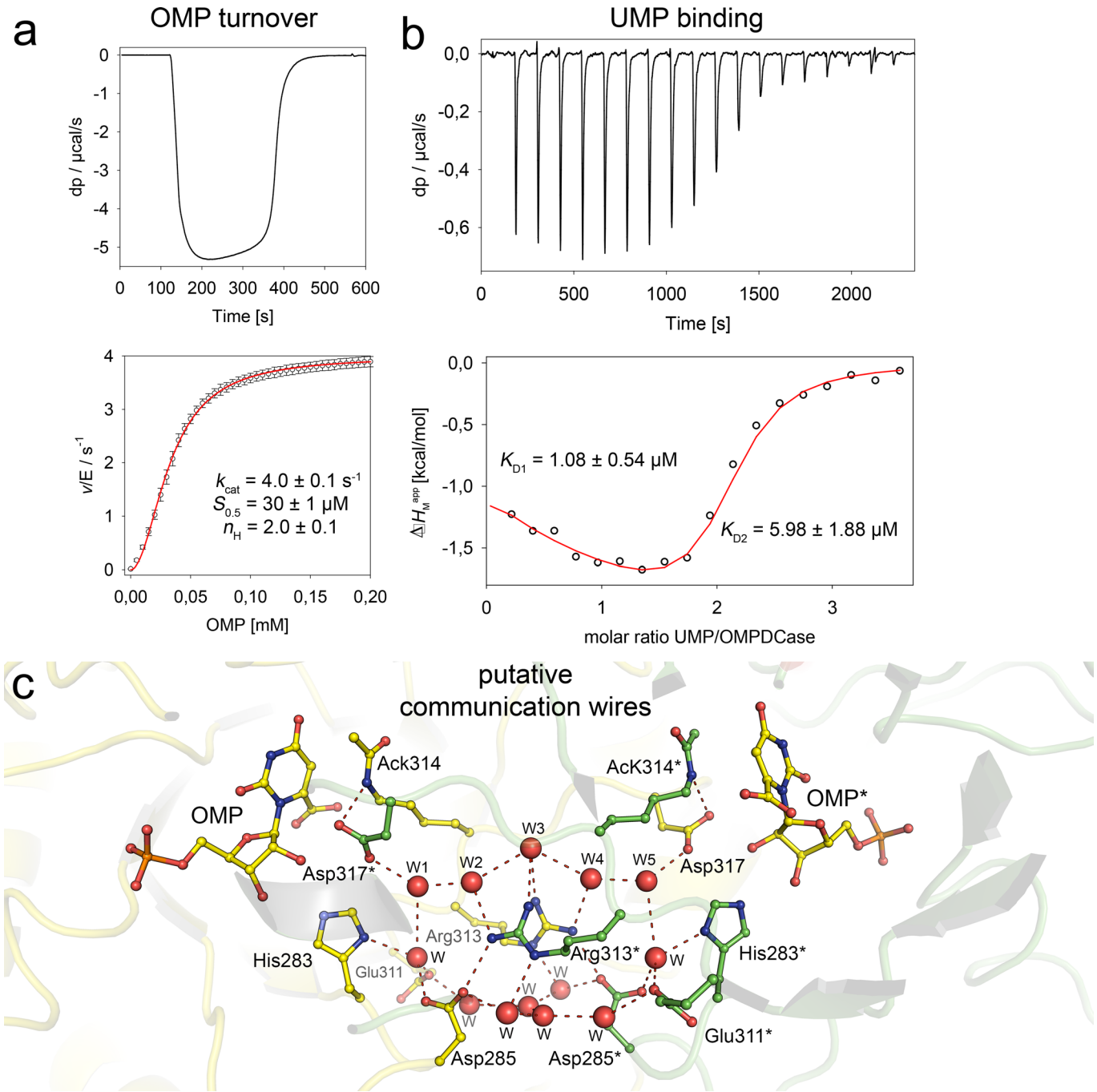

Extended Data Fig. 6 | Detection of cooperativity in human OMPDC catalysis. Detection of cooperativity in human OMPDC catalysis. (**a**) Steady-state kinetic analysis of OMPDC-catalysed conversion of OMP into UMP by isothermal titration calorimetry showing the raw data thermogram after a single injection of 0.2 mM OMP to a solution containing 1 µM OMPDC in 20 mM HEPES/NaOH, pH 7.4 at 25 °C and the therefrom calculated v_S plot. The data were fitted with the Hill equation (fit shown in red). Note the estimated Hill coefficient of $n_H = 2.0$ that indicates positive cooperativity between the two active sites in the homodimeric enzyme. All measurements were carried out in triplicate and are shown as mean ± s.d. (**b**) Thermodynamic analysis of binding of product UMP to human OMPDC using isothermal titration calorimetry showing the raw data thermogram and the integrated heats. The data were fit with a two-site binding model as detailed in the methods section (fit shown in red). The observation of two binding sites suggests a negative cooperativity between the two active sites in the homodimeric enzyme. All experiments were carried out as triplicates with almost identical results. The fitted kinetic and thermodynamic constants along with the associated calculated standard deviation are shown for a representative experiment. (**c**) Putative communication wires in human OMPCase that link the two remote active sites of the homodimer. Shown is the structure of human OMPDC variant Lys314AcLys in complex with substrate OMP highlighting the two active sites with the bound substrate molecules and two potential signaling pathways involving Asp317*-W1-W2-W3-W4-W5-Asp317 and/or His283-Glu311-Asp285 from both subunits and several water molecules. Abbreviations: OMPDC, orotidine-5′-monophosphate decarboxylase; OMP, orotidine-5′-monophosphate; UMP, uridine-5′-monophosphate.

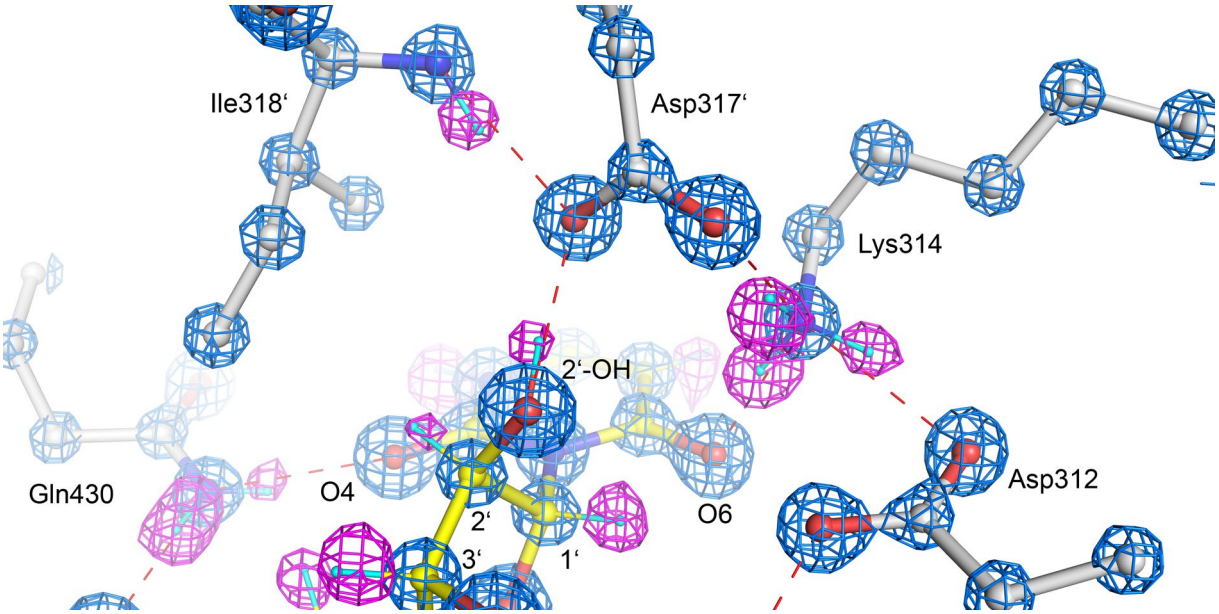

Extended Data Fig. 7 | Structure of human OMPDC in complex with transition-state analog BMP. Structure of human OMPDC in complex with transition-state analog BMP. Close-up of the active site showing the local interactions of residue Asp317′. The structural model is superposed with the corresponding 2mFo-DFc electron density map (blue, contour level 5.3σ). Peaks in the H-omit mFo-DFc difference electron density map (magenta, contour level 3σ) indicate the positions of hydrogen atoms of the analog and interacting protein groups. The structural data suggest that the side chain Asp317′ is ionized and interacts with Lys314 (-NH_3^+), the backbone amide of Ile318′ and the 2′-OH group of BMP. Crystallographic statistics are provided in Supplementary Table 1. Abbreviations: OMPDC, orotidine-5′-monophosphate decarboxylase; BMP, 6-hydroxy-UMP.

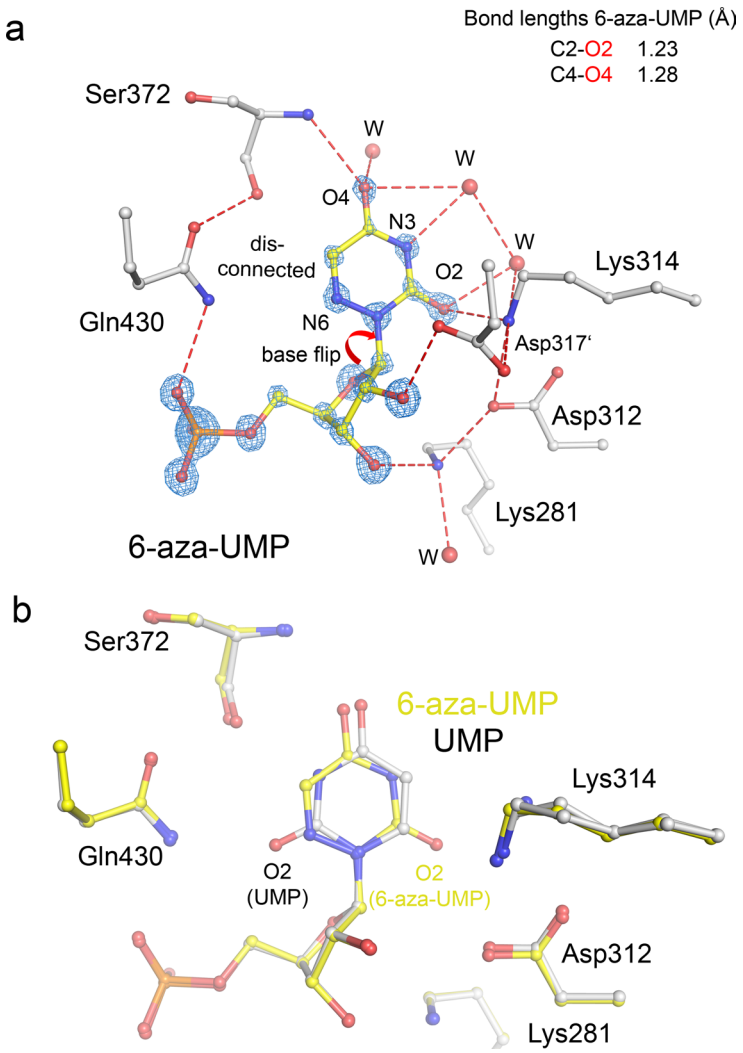

Extended Data Fig. 8 | Structure of human OMPDC in complex with transition-state analog 6-aza-UMP. Structure of human OMPDC in complex with transition-state analog 6-aza-UMP. (**a**) Close-up of the active site showing the bound analog, interacting protein groups and water molecules (W). Hydrogen bonds and the bond lengths of the C2-O2 and C4-O4 bonds are indicated. Note the *syn*-conformation of the base that places the 2-oxo group into the vicinity of the catalytic tetrad rather than Gln430 as observed for all other ligands, which bind in the *anti*-conformation (see panel b). The structural models are superposed with the corresponding 2mFo-DFc electron density maps at a contour level of 5.3σ (in blue). Crystallographic statistics are provided in Supplementary Table 1. (**b**) Structural superposition of OMPDC in complex with 6-aza-UMP (in yellow) and UMP (in grey) showing the active site including the bound ligand and selected active site residues. Note the different orientation of the the 2-oxo function for both ligands. Abbreviations: OMPDC, orotidine-5'-monophosphate decarboxylase; UMP, uridine-5'-monophosphate.

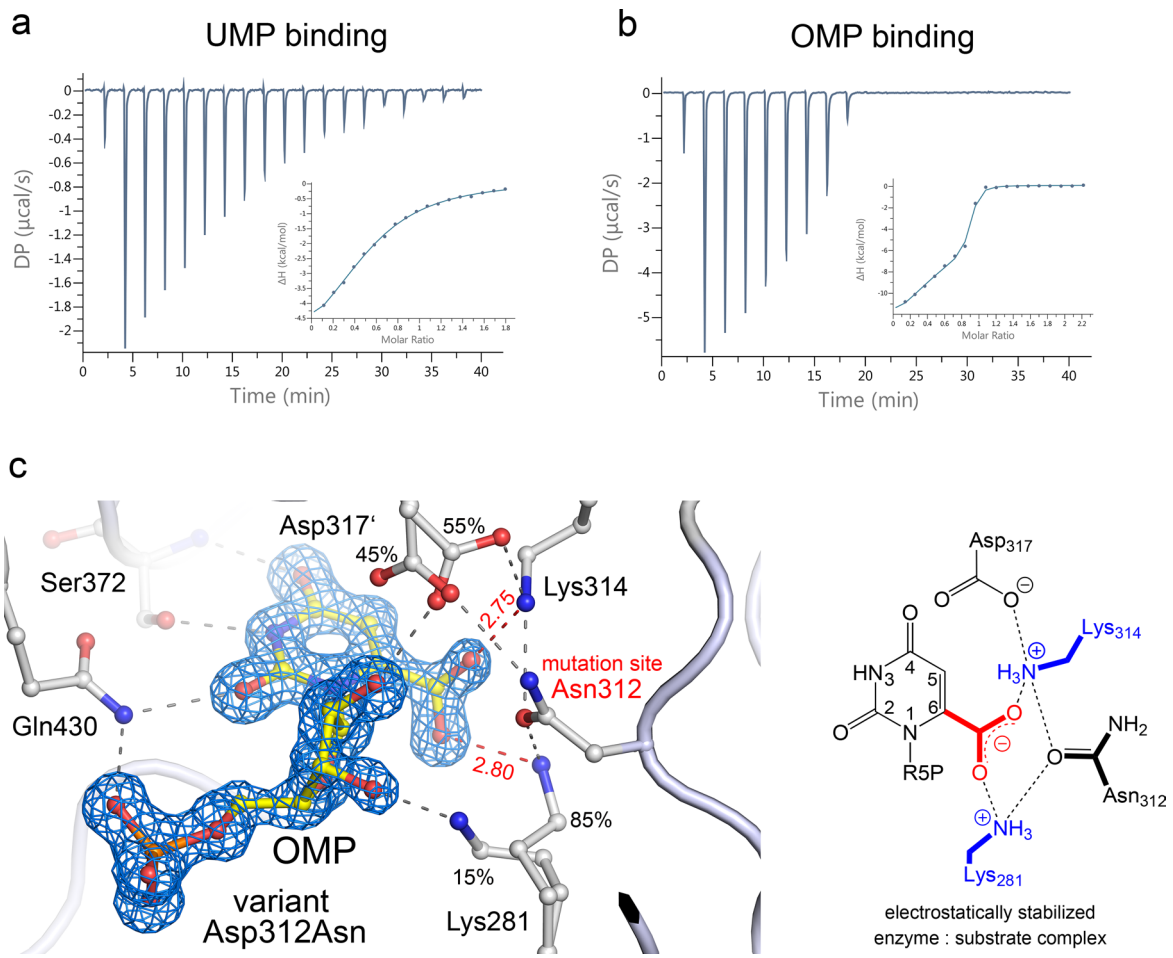

Extended Data Fig. 9 | Functional and structural analysis of human OMPDC variant Asp312Asn. Functional and structural analysis of human OMPDC variant Asp312Asn. The variant exhibits no measurable enzymatic activity for conversion of OMP. (**a**) Thermodynamic analysis of binding of product UMP to variant Asp312Asn using isothermal titration calorimetry showing the raw data thermogram and the integrated heats (inset). The data were fit with a 1:1 binding model and yielded a dissociation constant of K_D^{app} = 49 ± 6 µM and a stoichiometry *N* of 0.59 ± 0.01 indicative for half-of-the-sites reactivity. (**b**) Thermodynamic analysis of binding of substrate OMP to variant Asp312Asn using isothermal titration calorimetry showing the raw date thermogram and the integrated heats (inset). The data were fit with a two-sites binding model and yielded dissociation constants of K_D^1 = 0.58 ± 0.56 µM K_D^2 = 0.19 ± 0.09 µM indicative for positive cooperativity. (**c**) Structure of variant Asp312Asn in complex with substrate showing the active site with bound OMP and interacting residues. The structural model of OMP is superposed with the 2mFo-DFc electron density map (in blue) at a contour level of 2σ. Hydrogen-bond interactions of OMP with active-site residues and relative occupancies for residues with alternative conformations are indicated. Note that the carboxylate portion of OMP is interacting with both Lys281 as well as Lys314 forming a stable (anticatalytic) enzyme: substrate complex as shown in the accompanying scheme. All experiments were carried out as triplicates with almost identical results. The fitted kinetic and thermodynamic constants along with the associated calculated standard deviation are shown for a representative experiment. Crystallographic statistics are provided in Supplementary Table 1. Abbreviations: OMPDC, orotidine-5′-monophosphate decarboxylase; OMP, orotidine-5′-monophosphate; UMP, uridine-5′-monophosphate.

nature research

Corresponding author(s): Tittmann, Kai

Last updated by author(s): Feb 22, 2022

Reporting Summary

Nature Research wishes to improve the reproducibility of the work that we publish. This form provides structure for consistency and transparency in reporting. For further information on Nature Research policies, see Authors & Referees and the Editorial Policy Checklist.

Statistics

For all statistical analyses, confirm that the following items are present in the figure legend, table legend, main text, or Methods section.

n/a	Confirmed	
☐	☒	The exact sample size (*n*) for each experimental group/condition, given as a discrete number and unit of measurement
☒	☐	A statement on whether measurements were taken from distinct samples or whether the same sample was measured repeatedly
☒	☐	The statistical test(s) used AND whether they are one- or two-sided *Only common tests should be described solely by name; describe more complex techniques in the Methods section.*
☒	☐	A description of all covariates tested
☒	☐	A description of any assumptions or corrections, such as tests of normality and adjustment for multiple comparisons
☐	☒	A full description of the statistical parameters including central tendency (e.g. means) or other basic estimates (e.g. regression coefficient) AND variation (e.g. standard deviation) or associated estimates of uncertainty (e.g. confidence intervals)
☒	☐	For null hypothesis testing, the test statistic (e.g. *F*, *t*, *r*) with confidence intervals, effect sizes, degrees of freedom and *P* value noted *Give P values as exact values whenever suitable.*
☒	☐	For Bayesian analysis, information on the choice of priors and Markov chain Monte Carlo settings
☒	☐	For hierarchical and complex designs, identification of the appropriate level for tests and full reporting of outcomes
☒	☐	Estimates of effect sizes (e.g. Cohen's *d*, Pearson's *r*), indicating how they were calculated

Our web collection on statistics for biologists contains articles on many of the points above.

Software and code

Policy information about availability of computer code

Data collection	Kinetics and spectroscopic analysis Spectra Manager version 2.07.02 (Build 4) (UV-Vis-based Kinetics) Isothermal calorimetry MicroCal PEAQ-ITC Software 1.21 X-ray crystallography mxCuBE 2 (X-ray data collection at P14 DESY/EMBL, Hamburg, Germany) Computational Chemistry Python3.1 (libraries: numpy, matplotlib) Gaussian16 RevA.03 (molecular electrostatic potentials) Orca 4.0.1 (DFT calculations for energy scans and DFT/MM calculations) Chemshell 3.5.0 (interface for DFT/MM optimisations and energy calculations) Amber 18.11 (molecular dynamics, molecular mechanics, DFTB calculations) AmberTools 18.12 (system preparation, force field fitting) WHAM 2.0.9 (calculation of potential of mean force from constrained molecular dynamics)
Data analysis	Kinetics and spectroscopic analysis Spectra Manager version 2.07.02 (Build 4) (UV-Vis-based Kinetics) SigmaPlot version 11.0 (UV-Vis- and ITC-based Kinetics) Isothermal calorimetry MicroCal PEAQ-ITC Software 1.21

Nitpic version 1.2.7
ITCsy version 1.0a

Crystallography
XDS VERSION Mar 15, 2019 BUILT=20190315 (X-ray, data processing)
XSCALE VERSION Jan 31, 2020 BUILT=20200417 (X-ray, data scaling)
CCP4 version 7.0.78 (X-ray, processing and refinement)
autoPROC version 1.05 (X-ray, data processing and scaling)
phenix.refine version 1.17.1_3660 (structure, refinement)
REFMAC5 version 5.8.0258 (structure, refinement)
SHELXL version 2019 (structure, refinement)
COOT version 0.8.9.1 (structure, model building)
MolProbity-Server Version 4 (structure validation)
The PyMOL Molecular Graphics System version 1.3 (structure representation)

Computational Chemistry
Python3.1 (libraries: numpy, matplotlib)
Gaussian16 RevA.03 (molecular electrostatic potentials)
Orca 4.0.1 (DFT calculations for energy scans and DFT/MM calculations)
Chemshell 3.5.0 (interface for DFT/MM optimisations and energy calculations)
Amber 18.11 (molecular dynamics, molecular mechanics, DFTB calculations)
AmberTools 18.12 (system preparation, force field fitting)
WHAM 2.0.9 (calculation of potential of mean force from constrained molecular dynamics)

For manuscripts utilizing custom algorithms or software that are central to the research but not yet described in published literature, software must be made available to editors/reviewers. We strongly encourage code deposition in a community repository (e.g. GitHub). See the Nature Research guidelines for submitting code & software for further information.

Data

Policy information about availability of data

All manuscripts must include a data availability statement. This statement should provide the following information, where applicable:

- Accession codes, unique identifiers, or web links for publicly available datasets
- A list of figures that have associated raw data
- A description of any restrictions on data availability

The refined structural protein models and corresponding structure-factor amplitudes are deposited under PDB accession codes 7OUZ (Wild type, BMP, crystal 1), 7OTU (Wild type, BMP, crystal 2), 6ZWY (Wild type, UMP), 6ZX1 (Wild type, Aza-UMP), 7OV0 (Wild type, ground state), 6ZX2 (Carboxamido-UMP), 6ZX3 (Thiocarboxamido-UMP), 7ASQ (Wild type, UMP), 6ZWZ (314AcK, ground state), 6YWU (314AcK, UMP), 6YVK (314AcK, 2 min soaking with OMP, 0.71 MGy dose), 6YVL (314AcK, 2 min soaking with OMP, 1.42 MGy dose), 6YVM (314AcK, 2 min soaking with OMP, 2.13 MGy dose), 6YVN (K314AcK, 2 min soaking with OMP, 2.84 MGy dose), 6YVO (K314AcK, 2 min soaking with OMP, 3.55 MGy dose), 6YWT (K314AcK, BMP), 7OQF (K314AcK, 5 min soaking with OMP), 7OQI (K314AcK, 10 min soaking with OMP), 7OQK (K314AcK, 15 min soaking with OMP), 7OQM (K314AcK, 20 min soaking with OMP), 7OQN (K314AcK, 30 min soaking with OMP), 7AM9 (K314AcK, 2 min soaking with OMP, merged dataset), 6ZX0 (K314AcK, OMP), 7Q1H (D312N, 2 min soak OMP). All other data are available on request.

Field-specific reporting

Please select the one below that is the best fit for your research. If you are not sure, read the appropriate sections before making your selection.

☒ Life sciences ☐ Behavioural & social sciences ☐ Ecological, evolutionary & environmental sciences

For a reference copy of the document with all sections, see nature.com/documents/nr-reporting-summary-flat.pdf

Life sciences study design

All studies must disclose on these points even when the disclosure is negative.

Sample size	This study did not involve a sample analysis.
Data exclusions	No data were excluded.
Replication	All functional analyses were carried out as triplicates (n=3), the resulting mean +/- standard deviation are shown as error bars. Fitting of the data yielded standard errors for all estimated parameters.
Randomization	not applicable as this study did not involve a sample analysis.
Blinding	not applicable as this study did not involve a sample analysis.

Behavioural & social sciences study design

All studies must disclose on these points even when the disclosure is negative.

Study description	*Briefly describe the study type including whether data are quantitative, qualitative, or mixed-methods (e.g. qualitative cross-sectional, quantitative experimental, mixed-methods case study).*
Research sample	*State the research sample (e.g. Harvard university undergraduates, villagers in rural India) and provide relevant demographic information (e.g. age, sex) and indicate whether the sample is representative. Provide a rationale for the study sample chosen. For studies involving existing datasets, please describe the dataset and source.*
Sampling strategy	*Describe the sampling procedure (e.g. random, snowball, stratified, convenience). Describe the statistical methods that were used to predetermine sample size OR if no sample-size calculation was performed, describe how sample sizes were chosen and provide a rationale for why these sample sizes are sufficient. For qualitative data, please indicate whether data saturation was considered, and what criteria were used to decide that no further sampling was needed.*
Data collection	*Provide details about the data collection procedure, including the instruments or devices used to record the data (e.g. pen and paper, computer, eye tracker, video or audio equipment) whether anyone was present besides the participant(s) and the researcher, and whether the researcher was blind to experimental condition and/or the study hypothesis during data collection.*
Timing	*Indicate the start and stop dates of data collection. If there is a gap between collection periods, state the dates for each sample cohort.*
Data exclusions	*If no data were excluded from the analyses, state so OR if data were excluded, provide the exact number of exclusions and the rationale behind them, indicating whether exclusion criteria were pre-established.*
Non-participation	*State how many participants dropped out/declined participation and the reason(s) given OR provide response rate OR state that no participants dropped out/declined participation.*
Randomization	*If participants were not allocated into experimental groups, state so OR describe how participants were allocated to groups, and if allocation was not random, describe how covariates were controlled.*

Ecological, evolutionary & environmental sciences study design

All studies must disclose on these points even when the disclosure is negative.

Study description	*Briefly describe the study. For quantitative data include treatment factors and interactions, design structure (e.g. factorial, nested, hierarchical), nature and number of experimental units and replicates.*
Research sample	*Describe the research sample (e.g. a group of tagged Passer domesticus, all Stenocereus thurberi within Organ Pipe Cactus National Monument), and provide a rationale for the sample choice. When relevant, describe the organism taxa, source, sex, age range and any manipulations. State what population the sample is meant to represent when applicable. For studies involving existing datasets, describe the data and its source.*
Sampling strategy	*Note the sampling procedure. Describe the statistical methods that were used to predetermine sample size OR if no sample-size calculation was performed, describe how sample sizes were chosen and provide a rationale for why these sample sizes are sufficient.*
Data collection	*Describe the data collection procedure, including who recorded the data and how.*
Timing and spatial scale	*Indicate the start and stop dates of data collection, noting the frequency and periodicity of sampling and providing a rationale for these choices. If there is a gap between collection periods, state the dates for each sample cohort. Specify the spatial scale from which the data are taken*
Data exclusions	*If no data were excluded from the analyses, state so OR if data were excluded, describe the exclusions and the rationale behind them, indicating whether exclusion criteria were pre-established.*
Reproducibility	*Describe the measures taken to verify the reproducibility of experimental findings. For each experiment, note whether any attempts to repeat the experiment failed OR state that all attempts to repeat the experiment were successful.*
Randomization	*Describe how samples/organisms/participants were allocated into groups. If allocation was not random, describe how covariates were controlled. If this is not relevant to your study, explain why.*
Blinding	*Describe the extent of blinding used during data acquisition and analysis. If blinding was not possible, describe why OR explain why blinding was not relevant to your study.*

Did the study involve field work? ☐ Yes ☐ No

Field work, collection and transport

Field conditions	*Describe the study conditions for field work, providing relevant parameters (e.g. temperature, rainfall).*
Location	*State the location of the sampling or experiment, providing relevant parameters (e.g. latitude and longitude, elevation, water depth).*
Access and import/export	*Describe the efforts you have made to access habitats and to collect and import/export your samples in a responsible manner and in compliance with local, national and international laws, noting any permits that were obtained (give the name of the issuing authority, the date of issue, and any identifying information).*
Disturbance	*Describe any disturbance caused by the study and how it was minimized.*

Reporting for specific materials, systems and methods

We require information from authors about some types of materials, experimental systems and methods used in many studies. Here, indicate whether each material, system or method listed is relevant to your study. If you are not sure if a list item applies to your research, read the appropriate section before selecting a response.

Materials & experimental systems

n/a	Involved in the study
☒	☐ Antibodies
☒	☐ Eukaryotic cell lines
☒	☐ Palaeontology
☒	☐ Animals and other organisms
☒	☐ Human research participants
☒	☐ Clinical data

Methods

n/a	Involved in the study
☒	☐ ChIP-seq
☒	☐ Flow cytometry
☒	☐ MRI-based neuroimaging

Antibodies

Antibodies used	*Describe all antibodies used in the study; as applicable, provide supplier name, catalog number, clone name, and lot number.*
Validation	*Describe the validation of each primary antibody for the species and application, noting any validation statements on the manufacturer's website, relevant citations, antibody profiles in online databases, or data provided in the manuscript.*

Eukaryotic cell lines

Policy information about cell lines

Cell line source(s)	*State the source of each cell line used.*
Authentication	*Describe the authentication procedures for each cell line used OR declare that none of the cell lines used were authenticated.*
Mycoplasma contamination	*Confirm that all cell lines tested negative for mycoplasma contamination OR describe the results of the testing for mycoplasma contamination OR declare that the cell lines were not tested for mycoplasma contamination.*
Commonly misidentified lines (See ICLAC register)	*Name any commonly misidentified cell lines used in the study and provide a rationale for their use.*

Palaeontology

Specimen provenance	*Provide provenance information for specimens and describe permits that were obtained for the work (including the name of the issuing authority, the date of issue, and any identifying information).*
Specimen deposition	*Indicate where the specimens have been deposited to permit free access by other researchers.*
Dating methods	*If new dates are provided, describe how they were obtained (e.g. collection, storage, sample pretreatment and measurement), where they were obtained (i.e. lab name), the calibration program and the protocol for quality assurance OR state that no new dates are provided.*

☐ Tick this box to confirm that the raw and calibrated dates are available in the paper or in Supplementary Information.

Animals and other organisms

Policy information about studies involving animals; ARRIVE guidelines recommended for reporting animal research

Laboratory animals	*For laboratory animals, report species, strain, sex and age OR state that the study did not involve laboratory animals.*
Wild animals	*Provide details on animals observed in or captured in the field; report species, sex and age where possible. Describe how animals were caught and transported and what happened to captive animals after the study (if killed, explain why and describe method; if released, say where and when) OR state that the study did not involve wild animals.*
Field-collected samples	*For laboratory work with field-collected samples, describe all relevant parameters such as housing, maintenance, temperature, photoperiod and end-of-experiment protocol OR state that the study did not involve samples collected from the field.*
Ethics oversight	*Identify the organization(s) that approved or provided guidance on the study protocol, OR state that no ethical approval or guidance was required and explain why not.*

Note that full information on the approval of the study protocol must also be provided in the manuscript.

Human research participants

Policy information about studies involving human research participants

Population characteristics	*Describe the covariate-relevant population characteristics of the human research participants (e.g. age, gender, genotypic information, past and current diagnosis and treatment categories). If you filled out the behavioural & social sciences study design questions and have nothing to add here, write "See above."*
Recruitment	*Describe how participants were recruited. Outline any potential self-selection bias or other biases that may be present and how these are likely to impact results.*
Ethics oversight	*Identify the organization(s) that approved the study protocol.*

Note that full information on the approval of the study protocol must also be provided in the manuscript.

Clinical data

Policy information about clinical studies

All manuscripts should comply with the ICMJE guidelines for publication of clinical research and a completed CONSORT checklist must be included with all submissions.

Clinical trial registration	*Provide the trial registration number from ClinicalTrials.gov or an equivalent agency.*
Study protocol	*Note where the full trial protocol can be accessed OR if not available, explain why.*
Data collection	*Describe the settings and locales of data collection, noting the time periods of recruitment and data collection.*
Outcomes	*Describe how you pre-defined primary and secondary outcome measures and how you assessed these measures.*

ChIP-seq

Data deposition

☐ Confirm that both raw and final processed data have been deposited in a public database such as GEO.

☐ Confirm that you have deposited or provided access to graph files (e.g. BED files) for the called peaks.

Data access links *May remain private before publication.*	*For "Initial submission" or "Revised version" documents, provide reviewer access links. For your "Final submission" document, provide a link to the deposited data.*
Files in database submission	*Provide a list of all files available in the database submission.*
Genome browser session (e.g. UCSC)	*Provide a link to an anonymized genome browser session for "Initial submission" and "Revised version" documents only, to enable peer review. Write "no longer applicable" for "Final submission" documents.*

Methodology

Replicates	*Describe the experimental replicates, specifying number, type and replicate agreement.*
Sequencing depth	*Describe the sequencing depth for each experiment, providing the total number of reads, uniquely mapped reads, length of reads and whether they were paired- or single-end.*
Antibodies	*Describe the antibodies used for the ChIP-seq experiments; as applicable, provide supplier name, catalog number, clone*

Antibodies	*name, and lot number.*
Peak calling parameters	*Specify the command line program and parameters used for read mapping and peak calling, including the ChIP, control and index files used.*
Data quality	*Describe the methods used to ensure data quality in full detail, including how many peaks are at FDR 5% and above 5-fold enrichment.*
Software	*Describe the software used to collect and analyze the ChIP-seq data. For custom code that has been deposited into a community repository, provide accession details.*

Flow Cytometry

Plots

Confirm that:

☐ The axis labels state the marker and fluorochrome used (e.g. CD4-FITC).

☐ The axis scales are clearly visible. Include numbers along axes only for bottom left plot of group (a 'group' is an analysis of identical markers).

☐ All plots are contour plots with outliers or pseudocolor plots.

☐ A numerical value for number of cells or percentage (with statistics) is provided.

Methodology

Sample preparation	*Describe the sample preparation, detailing the biological source of the cells and any tissue processing steps used.*
Instrument	*Identify the instrument used for data collection, specifying make and model number.*
Software	*Describe the software used to collect and analyze the flow cytometry data. For custom code that has been deposited into a community repository, provide accession details.*
Cell population abundance	*Describe the abundance of the relevant cell populations within post-sort fractions, providing details on the purity of the samples and how it was determined.*
Gating strategy	*Describe the gating strategy used for all relevant experiments, specifying the preliminary FSC/SSC gates of the starting cell population, indicating where boundaries between "positive" and "negative" staining cell populations are defined.*

☐ Tick this box to confirm that a figure exemplifying the gating strategy is provided in the Supplementary Information.

Magnetic resonance imaging

Experimental design

Design type	*Indicate task or resting state; event-related or block design.*
Design specifications	*Specify the number of blocks, trials or experimental units per session and/or subject, and specify the length of each trial or block (if trials are blocked) and interval between trials.*
Behavioral performance measures	*State number and/or type of variables recorded (e.g. correct button press, response time) and what statistics were used to establish that the subjects were performing the task as expected (e.g. mean, range, and/or standard deviation across subjects).*

Acquisition

Imaging type(s)	*Specify: functional, structural, diffusion, perfusion.*
Field strength	*Specify in Tesla*
Sequence & imaging parameters	*Specify the pulse sequence type (gradient echo, spin echo, etc.), imaging type (EPI, spiral, etc.), field of view, matrix size, slice thickness, orientation and TE/TR/flip angle.*
Area of acquisition	*State whether a whole brain scan was used OR define the area of acquisition, describing how the region was determined.*

Diffusion MRI ☐ Used ☐ Not used

Preprocessing

Preprocessing software	*Provide detail on software version and revision number and on specific parameters (model/functions, brain extraction, segmentation, smoothing kernel size, etc.).*

Normalization

If data were normalized/standardized, describe the approach(es): specify linear or non-linear and define image types used for transformation OR indicate that data were not normalized and explain rationale for lack of normalization.

Normalization template

Describe the template used for normalization/transformation, specifying subject space or group standardized space (e.g. original Talairach, MNI305, ICBM152) OR indicate that the data were not normalized.

Noise and artifact removal

Describe your procedure(s) for artifact and structured noise removal, specifying motion parameters, tissue signals and physiological signals (heart rate, respiration).

Volume censoring

Define your software and/or method and criteria for volume censoring, and state the extent of such censoring.

Statistical modeling & inference

Model type and settings

Specify type (mass univariate, multivariate, RSA, predictive, etc.) and describe essential details of the model at the first and second levels (e.g. fixed, random or mixed effects; drift or auto-correlation).

Effect(s) tested

Define precise effect in terms of the task or stimulus conditions instead of psychological concepts and indicate whether ANOVA or factorial designs were used.

Specify type of analysis: ☐ Whole brain ☐ ROI-based ☐ Both

Statistic type for inference
(See Eklund et al. 2016)

Specify voxel-wise or cluster-wise and report all relevant parameters for cluster-wise methods.

Correction

Describe the type of correction and how it is obtained for multiple comparisons (e.g. FWE, FDR, permutation or Monte Carlo).

Models & analysis

n/a	Involved in the study
☐	☐ Functional and/or effective connectivity
☐	☐ Graph analysis
☐	☐ Multivariate modeling or predictive analysis

Functional and/or effective connectivity

Report the measures of dependence used and the model details (e.g. Pearson correlation, partial correlation, mutual information).

Graph analysis

Report the dependent variable and connectivity measure, specifying weighted graph or binarized graph, subject- or group-level, and the global and/or node summaries used (e.g. clustering coefficient, efficiency, etc.).

Multivariate modeling and predictive analysis

Specify independent variables, features extraction and dimension reduction, model, training and evaluation metrics.